

Maximilian SCHINAGL BSc

Localising Ferritin and Iron in Human Brain Tissue using Immuno-Electron Microscopy

MASTER'S THESIS

to achieve the university degree of
Master of Science

Master's degree programme:
Biochemistry and Molecular Biomedical Sciences

submitted to

Graz University of Technology

Supervisor

Assoz. Prof. Priv.-Doz. Mag. Dr.rer.nat. Gerd LEITINGER

Gottfried Schatz Research Center for Cell Signalling, Metabolism and Ageing
Department of Cell Biology, Histology and Embryology

Research Unit Electron Microscopic Techniques
Co-Supervisor: Mariella SELE MSc

Graz, August 2018

This document is set in Palatino, compiled with pdfL^AT_EX₂ε and Biber.
The L^AT_EX template from Karl Voit is based on KOMA script and can be found
online: <https://github.com/novoid/LaTeX-KOMA-template>

Affidavit

I declare that I have authored this thesis independently, that I have not used other than the declared sources/resources, and that I have explicitly indicated all material which has been quoted either literally or by content from the sources used. The text document uploaded to TUGRAZonline is identical to the present master's thesis.

Graz, August 9th 2018

Location, Date

A handwritten signature in black ink, written over a horizontal line. The signature is cursive and appears to read 'M. Glunz'.

Signature

Für Muttl und Chef

Thank you to all the team members of the Research Unit Electron Microscopic Techniques for providing such great assistance during my thesis.

Thank you to all my parents for their emotional and financial support during all these years. I would not be where I am now without your guidance and encouragement.

Thank you to all my friends and fellow students for giving me the best time in my life so far.

Abstract

Background & aim: Iron overload in the human brain has been reported to play an essential role in many neurodegenerative diseases, including Alzheimer's. A causal relationship between this excessive iron deposition and the appearance of neurodegenerative diseases has not yet been discovered. The difference in iron load between different brain regions and between different cell types within these regions, as well as differences in the iron storage mechanism in these areas is mostly unknown and is pre-requisite for understanding the role iron plays in neurodegenerative diseases.

The most important iron storage protein in the human brain is ferritin. Localising ferritin and iron deposits within ferritin at a sub-cellular level will thus offer unprecedented insight into the distribution and storage characteristics of iron. This will be an important step towards understanding the relation between iron tissue deposition and neurodegenerative diseases. The aim of this thesis was to establish a workflow combining (i) immunogold labelling of ferritin, in order to localise ferritin on electron micrographs, with (ii) analytical electron microscopy, in order to localise the iron deposits within the ferritin particles.

Method: In thin slices of chemically fixed human brain tissue, ferritin is tagged with a 10 nm gold particle, which is easily identifiable in a transmission electron microscope (TEM). Large, random areas of the sample are analysed for their ferritin content by indirectly localising ferritin through the gold particles. These gold particles are automatically identified and counted, using image analysis software.

The tagging of ferritin proteins is reviewed by analysing the elemental composition of ferritin-gold particle pairs. This analysis is done with two independent TEM techniques, energy filtered transmission electron microscopy (EFTEM) and energy dispersive X-ray analysis (EDX).

Results & conclusion: After several attempted improvements of sample preparation protocols, a workflow could be introduced which is capable of reliably identifying ferritin in large areas of tissue samples. Using both EFTEM and EDX, the iron core of ferritin could be observed to be in close proximity to gold particles on multiple occasions. The workflow proposed in this thesis allows the accurate localisation of ferritin and its iron core in human brain tissue.

Outlook: The workflow introduced in this thesis enables a specific analysis of the ferritin distribution in large areas of brain tissue. This will allow a comparison of ferritin distributions in healthy and diseased brain tissue in future experiments. Moreover, the distribution of ferritin can be correlated to the distribution of iron in the human brain.

Significance: The workflow proposed in this thesis offers the quantification and localisation of ferritin on a cellular and sub-cellular, as well as a tissue specific level. The unique feature of this workflow is the reliability of the detection.

Zusammenfassung

Grundlagen und Ziele: Neurodegenerative Erkrankungen wie z. B. Alzheimer stehen in enger Verbindung mit erhöhter Eisenablagerung im menschlichen Gehirn. Ein kausaler Zusammenhang zwischen dieser vermehrten Ablagerung von Eisen, und dem Auftreten neurodegenerativer Erkrankungen konnte noch nicht mit Sicherheit festgestellt werden. Die Darstellung dieses Umstandes ist eine wesentliche Voraussetzung für das Verständnis dieses Zusammenhangs.

Ferritin ist das wichtigste Eisenspeicherprotein im menschlichen Gehirn. Die Darstellung von Ferritin und dessen Eiseneinlagerungen mittels Elektronenmikroskopie wird also neue Erkenntnisse im Bereich der Verteilung und Speicherung von Eisen liefern. Dazu muss Ferritin sowohl auf der zellulären, als auch auf der subzellulären Ebene dargestellt werden. Hierfür ist die Kombination zweier Methoden notwendig: einerseits muss Ferritin mittels Immunogold lokalisiert werden, andererseits muss mittels analytischer Elektronenmikroskopie die Eiseneinlagerung innerhalb der Ferritinproteine dargestellt werden. In der vorliegenden Arbeit wurde ein Workflow entwickelt, der diese beiden Methoden miteinander kombiniert. Dies könnte dabei helfen, manche Mechanismen neurodegenerativer Erkrankungen und deren Beziehung zu Eisenablagerungen im menschlichem Gehirn besser zu verstehen.

Methode: Ferritin wird auf fixierten Gewebeproben menschlichen Gehirns mit einem 10 nm großen Goldpartikel markiert, welcher im Transmissionselektronenmikroskop (TEM) einfach nachzuweisen ist. Große, zufällig ausgewählte Probenbereiche werden indirekt auf ihren Ferritingehalt analysiert, indem die Goldpartikel nachgewiesen werden. Diese Partikel können mithilfe von Bildanalyse Software automatisch detektiert und gezählt werden.

Die Stichhaltigkeit dieser Markierung wird überprüft, indem eine Elementaranalyse dieser Ferritin-Goldpartikel Paare mithilfe spezieller TEM Techniken, der Energiegefilterten Transmissionselektronenmikroskopie (EFTEM) und der Energiedispersiven Röntgenspektroskopie (EDX) durchgeführt wird.

Ergebnisse und Conclusio: Nach mehreren Versuchen die Probenvorbereitung zu optimieren, konnte ein Workflow etabliert werden, welcher Ferritin in großen Gewebeteilen verlässlich nachweisen kann. Die Markierung des Ferritins konnte mit negativen Kontrollen, EFTEM und EDX überprüft, und an mehreren Stellen bestätigt werden.

Der vorgestellte Workflow erlaubt die akkurate Lokalisierung und Quantifizierung von Ferritin in Proben menschlichen Gehirns. Die Markierung des Ferritins mit einem Goldpartikel konnte direkt beobachtet werden.

Ausblick: Der Vergleich der Ferritin Distribution in krankem und gesundem Gewebe kann mit dem hier vorgestellten Workflow erfolgen. Des Weiteren kann die Ferritin Verteilung ebenfalls mit Eisenablagerungen im Gehirn verglichen werden.

Signifikanz: Der Workflow, welcher in dieser Arbeit vorgestellt wird, bietet

die Quantifizierung und Lokalisierung von Ferritin auf einer zellulären, subzellulären und auch gewebeweiten Ebene. Was diesen Workflow einzigartig macht, ist die Verlässlichkeit der Detektion, sowie die detaillierte Analyse der Ferritin Distribution.

Contents

Abstract	vii
1 Introduction	1
1.1 Iron in the human brain	1
1.1.1 The role of iron in neurodegenerative diseases	1
1.1.2 Current state of research	3
1.2 Finding iron in the human brain	4
1.2.1 Imaging of ferritin	4
1.3 Analytical electron microscopy	5
2 Methods	7
2.1 Sample preparation	7
2.1.1 Fixation of samples	8
2.1.2 Enhancing the contrast	9
2.1.3 Embedding of samples	10
2.1.4 Microtome sectioning	10
2.2 Immunogold labelling	11
2.2.1 Negative controls	13
2.2.2 Contrasting	14
2.3 Transmission electron microscopy	16
2.3.1 Transmission electron microscopy basics	16
2.3.2 Transmission electron microscopy operation	17
2.4 Image Analysis	17
2.5 Analytical electron microscopy	19
2.5.1 Analytical electron microscopy basics	19
2.5.2 Energy Filtered Transmission Electron Microscopy	19
2.5.3 Energy dispersive X-Ray analysis (EDX)	20
3 Results	23
3.1 Fixation and embedding refinement	23
3.1.1 Optimal fixation procedure	23
3.1.2 LR-white embedding refinements	25
3.2 Immunogold labelling	26
3.2.1 Primary antibody results	27
3.2.2 Negative controls	27
3.3 Contrasting	28
3.3.1 Heavily stained tissue results	28
3.3.2 Mildly stained tissue results	29

3.4	TEM image acquisition	29
3.4.1	Acquiring images of heavily stained tissue	29
3.4.2	Acquiring images of mildly stained tissue	29
3.5	Analytical electron microscopy results	32
3.5.1	EFTEM results	33
3.5.2	EDX results	33
4	Discussion	37
4.1	Fixation and embedding refinement	37
4.1.1	Optimal fixation and embedding procedure	37
4.2	Immunogold labelling	38
4.2.1	Detecting ferritin in heavily stained tissue	38
4.2.2	Detecting ferritin in mildly stained tissue	39
4.2.3	Negative Controls	40
4.3	Analytical EM	40
4.4	Conclusion	41
4.5	Outlook	41
5	Experimental	43
5.1	Sample Preparation	43
5.1.1	Fixation	43
5.1.2	LR-White Embedding	44
5.1.3	Specimen sectioning	44
5.1.4	Immunogold labelling	44
5.1.5	Sample Staining	45
5.2	Transmission Electron Microscopy	45
5.2.1	Image acquisition	45
5.3	Image Analysis	45
5.4	Analytical EM	46
5.4.1	Energy filtered transmission electron microscopy	46
5.4.2	Energy dispersive X-ray analysis	46
A	Materials	49
B	Addendum	51
B.1	Code	51
	Bibliography	53

List of Figures

1.1	Ferritin structure	2
1.2	Human brain	3
2.1	Sample preparation*	8
2.2	Ultramicrotome and glass knife*	11
2.3	Sectioning procedure*	12
2.4	Immuno labelling	12
2.5	Immuno labelling procedure	14
2.6	Contrasting chemicals	15
2.7	Transmission electron microscope	18
2.8	EFTEM and EDX	22
3.1	PIPES fixation test	24
3.2	Testing OsO ₄ for contrast enhancement	25
3.3	Absolute EtOH for fixation	26
3.4	Primary antibody dilution test results	27
3.5	Cell identification	30
3.6	Stitching of images using <i>SerialEM</i>	31
3.7	Automated gold counting	32
3.8	Ferritin detected per brain region	32
3.9	EFTEM images M-edge, L-edge and unfiltered	34
3.10	EDX measurements	35
4.1	Causes for unlabelled ferritin	41

Credit to Manuel Hündler for providing photographs (*)

Abbreviations

AD	Alzheimer's disease
CCD	charge-coupled device
DMT ₁	divalent metal transporter 1
ddH ₂ O	double distilled H ₂ O
EDX	energy dispersive X-ray analysis
EELS	electron energy loss spectroscopy
EFTEM	energy filtered transmission electron microscopy
EM	electron microscope
EtOH	ethanol
eV	electron volt
FA	formaldehyde
FIJI	FIJI is just ImageJ
FWM	frontal white matter
GA	glutaraldehyde
GP	globus pallidus
HAADF	high-angle annular dark-field
IgG	Immunoglobulin G
LR white	London resin white
MRI	magnetic resonance imaging
m/v%	mass per volume
PB	phosphate buffer
PBS	phosphate buffered saline
PBG	phosphate buffered glycine solution
PD	Parkinson's disease
PIPES	piperazine-N,N'-bis(2-ethanesulfonic acid)
Put	putamen
ROS	reactive oxygen species
STEM	scanning transmission electron microscopy
TEM	transmission electron microscope

1. Introduction

Iron is an essential element for all known mammals and plants [1]. It is involved in many important metabolic and physiological processes in the body, ranging from oxygen binding in haemoglobin to mitochondrial oxidative phosphorylation [2, 3]. Around 2.5 g or 50 % of iron in the human body is found in red blood cells, much of the other half is securely stored in specialized proteins called ferritins [4]. These proteins ensure a constant supply of iron for important cellular processes as they buffer temporary iron shortages [5]. In some cases, iron storage gets out of control and leads to adverse consequences, which can be especially severe in the human brain.

1.1. Iron in the human brain

Many cellular processes, such as the synthesis of various neurotransmitters depend on the presence of iron [6]. Neuronal development also is tightly linked to the availability of iron, as demonstrated by the occurrence of cognitive impairment in children suffering from iron deficiency [7]. Low brain iron levels lead to incomplete myelination of axons in the brain [8], causing neuronal failure. Iron availability can therefore be categorized as an important factor, not only in the maintenance of a healthy brain, but also its construction. Even in adults, low brain iron levels are associated with various cognitive problems like the restless leg syndrome [9].

1.1.1. The role of iron in neurodegenerative diseases

Low iron levels in the body can temporarily arise and cause various complications. However, accumulation of iron in the brain with age is a naturally occurring process. This surprising event is visible by the fact that infants start with almost no iron in the brain, while high iron levels are quite commonly found in elderly people [10]. This accumulation of iron in brain tissue has been subject to numerous studies [11, 12]. However, interest in this aspect of neurology has mainly been sparked by the discovery of a link between excessive iron deposition in the brain and many neurodegenerative diseases like Parkinson's or multiple sclerosis [13–15], but especially Alzheimer's disease (AD) [16]. Even though increased iron levels in the brain are a common feature in ageing, iron accumulation reaches pathological levels in some of these neurodegenerative diseases. For example, iron was found directly associated with amyloid β plaques [17], protein agglomerations which are believed to be a main cause for AD [18].

The role of iron storage

Even though the correlation between increased brain iron levels and neurodegenerative diseases is strong [19], a substantial amount of information on this topic is still missing. It is unclear which cell types store which amount of iron, which parts of the cells are involved, and sub-cellular structures are close to the iron stores. This conjuncture becomes even more interesting if differences in these aspects could be discovered between healthy and diseased brains.

Moreover, iron acts in substantially different ways, depending on its oxidation status and location. Cytosolic Fe^{2+} is usually harmless for the cell, but Fe^{3+} can catalyse reactions which produce reactive oxygen species (ROS) [20]. These molecules have severe effects on cell function and viability, which can be devastating for neurons and other cells in the brain [21].

Ferritin is regulating iron levels

Ferritin can internalize iron from cytosolic Fe^{2+} via oxidation to Fe^{3+} . This mechanism is keeping cytosolic iron at a low level and therefore reducing the adverse effects of free roaming iron [5], which can turn into cytotoxic Fe^{3+} . The inside of a ferritin protein is filled with an iron core, which is composed of Fe^{3+} in a ferrihydrite $(\text{Fe}^{3+})_2\text{O}_3 \cdot 0.5 \text{H}_2\text{O}$ configuration [22] and can store up to 4500 iron atoms [23]. This iron core is surrounded by a 1 nm thick protein hull, which is made from two distinct, self-assembling subunits. A representation of ferritin can be seen in Figure 1.1.

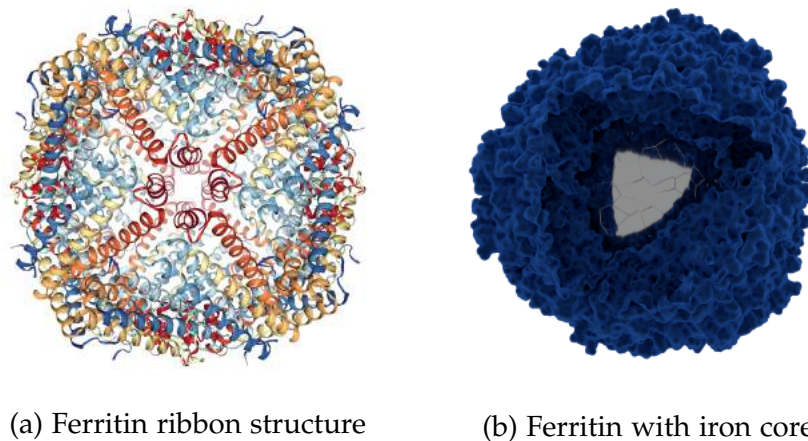


Figure 1.1.: The structure of ferritin. Image **a** shows the make-up of H-chain ferritin, where the subunits are presented in a ribbon structure. In the centre is a port where iron can enter and exit ferritin. Image **b** shows a rendered image of ferritin where part of the protein hull is removed for illustrative purposes. In the centre of the protein, an iron core can be seen. Both images are adapted from the protein data bank (*PDB* rcsb.org [24]) with some adjustments.

Even though ferritin is found throughout the human body, it is speculated that H-chain ferritin, which is primarily found in the brain, is specialized in fast iron uptake and release [25]. This quick uptake and release of iron in the brain is made possible by a high number of H-chain (heavy-chain) subunits, which are

specialized in this task. Up to 20 out of 24 subunits used to construct a ferritin protein in the brain are H-chain subunits, whereas liver ferritin utilizes only two to three H-chain subunits for its construction [26]. The remaining subunits are L-chain (light-chain), which are responsible for proper storage of iron [27]. Mutations in these H- and L-chain have been found to cause uncontrolled iron release [28]. In conclusion, ferritin is a sphere-shaped, iron storing protein, around 12 nm in diameter with a 3 - 6.5 nm¹ iron core on its inside [22].

1.1.2. Current state of research

It is already known that iron loads differ between brain regions in healthy human brains [29]. Basal ganglia, a collection of nuclei located in the midbrain, contain approximately five to ten times more iron than the cerebral cortex [30]. The location of these brain regions can be seen in Figure 1.2. This difference in iron storage in the brain is not fully understood yet.

Studies in rats could show that oligodendrocytes, which are responsible for the myelination and support of axons, contain a bulk amount of iron found in the brain [31]. Furthermore, it is unclear if additional iron is stored in ferritins until these proteins are full, or if a moderate filling status of ferritin is preferred; current research points to the latter [32].

These questions offer an interesting field of study. Differences in iron storage and iron levels between brain regions may also be discovered in AD brain tissue. A study shining light on these differences could offer unprecedented insight into the link between iron overload and neurodegenerative diseases.

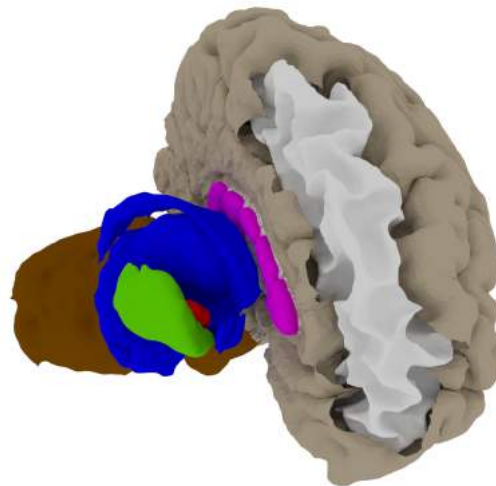


Figure 1.2.: Rendered image of a human brain. The cerebellum and grey matter are shown in brown and grey, respectively. The right hemisphere has been removed for illustrative purposes. Putamen and globus pallidus are shown in green and red, respectively. The rest of the basal ganglia nuclei are coloured in blue. Part of the left hemisphere, where some of the grey matter has been removed, shows the location of white matter. 3D files were acquired from *brainder.org* made possible by A. M. Winkler.

¹3 nm ferritin iron cores are mostly found in brain tissue, due to a lower number of L-chain subunits. 6.5 nm ferritin iron cores are mostly found in the liver.

1.2. Finding iron in the human brain

Electron microscopy (EM) can be used to elucidate the afore-stated questions, since this technique offers multiple ways to detect not only iron, but also ferritin on a cellular level. EM offers the possibility of detecting iron and ferritin and associating iron with ferritin. Furthermore, an automated system, allowing the identification of iron or ferritin, would further be able to identify the iron load and quantity of ferritin in a large sample size.

Our team has already shown that iron localisation with EM is possible in human brain tissue [33]. To follow up on the afore-stated importance of ferritin, this thesis is establishing a method to detect this important iron storage protein. Since a direct detection of ferritin with EM proves to be rather difficult, as will be discussed in the following section, an indirect approach is taken.

1.2.1. Imaging of ferritin

For an indirect localisation of ferritin, we are utilizing a method called immunogold labelling [34]. Arguably, it is possible to detect ferritin and the iron core on its inside directly using conventional EM. This has already been done as early as 1962 [35]. The ferritin protein hull cannot be detected in the microscope, but the iron-loaded ferritin is detectable, because of the strong electron density of the iron cores. However, dense proteins and agglomerations of proteins or other metals might be mistaken for ferritin iron cores quite easily. Furthermore, contrasted tissue, which will be needed for experiments performed in this thesis, renders this approach of ferritin iron core identification almost impossible. Automated identification of ferritin in this set up is also not feasible.

A conclusive study can only be done using a reliable method for the detection of ferritin. Therefore, a so-called indirect immunogold labelling approach, see Figure Figure 2.4 was used in this thesis, which is elaborated in more detail in section 2.2 *Immunogold labelling* on page 11. In brief, it consists of chemically fixing, dehydrating and embedding brain tissue in a special resin. Thin sections are made from preselected areas, and these sections are labelled with primary antibodies and gold-coupled secondary antibodies. This provides a highly selective localisation of ferritin in brain tissue.

Immunogold labelling is a well-established method in EM, which has been used for decades. It can accurately label small proteins, or even bigger structures that are hard to localise with other methods. Even though there are several ways of ensuring that the precise labelling of only the desired protein is taking place, see subsection 2.2.1 *Negative controls* on page 13, it is beneficial to have another level of conformation. It is also in our scientific interest to verify the specificity of labelling with a method different from the one used to produce positive results. Since our team is already using a method to localise iron cores of ferritin with analytical EM, we can use this method to confirm results produced from immunogold labelling.

1.3. Analytical electron microscopy

In this thesis, ferritin, a protein with an iron core on its inside, is marked with an antibody, tagged with a gold particle. Therefore, the gold particle should be found close to the ferritin iron core. Analytical EM includes several methods which were initially used in material science. The two methods used in this thesis are suited to correctly identify the elemental composition of small areas of tissue: Energy filtered transmission electron microscopy (EFTEM) and energy dispersive X-ray analysis (EDX), two independent methods, which are capable of correctly identifying the iron core and gold particle. A strong case for the validity of the immunogold labelling technique can be made, should these two particles be found close to each other.

In conclusion, this thesis introduces a workflow allowing the identification of the iron storing protein ferritin in human brain tissue. It uses immunogold labelling of ferritin to correctly localise this protein with EM. Automation, which will be introduced in subsection 2.3.2 *Transmission electron microscopy operation* on page 17, allows the identification of ferritin on a large scale. Analytical EM is used to confirm the correct labelling of ferritin with immunogold.

The number of ferritin proteins is analysed in three different regions of human brain tissue. Globus pallidus and putamen, both part of the basal ganglia, with suspected high amounts of ferritin and iron. Frontal white matter of the frontal cortex, a region in the brain with lower ferritin and iron content. In these three regions, ferritin is tagged with immunogold and for every gold particle that is found, one ferritin is counted. Random areas are chosen for the conformation of correct labelling with analytical EM.

2. Methods

In this thesis we are using human brain samples, in which ferritin proteins are labelled. This is done using immunogold, a small, but easily detectable gold particle, covalently linked to an antibody. A short summary of this process is given here and a more detailed explanation of every step involved in this procedure will be given in the subsequent sections. The project is kindly funded by the FWF (Austrian science fund) project number P 29370.

After receiving brain samples, they are chemically fixed and embedded as fast as possible, preventing the tissue from natural degradation. Finished samples are cut into thin sections with a thickness of ~ 70 nm. These thin sections are transferred onto copper grids, where immunogold labelling is done using specific anti-ferritin antibodies. After labelling, the sections are stained with heavy metals to enhance the contrast of structures in the sample. Later, these samples are observed in a transmission electron microscope (TEM), capable of detecting these small immunogold particles through their distinct strong electron density.

Images are acquired in a TEM when an electron beam passes through a thin sample and onto a camera. These images can then be analysed using image analysis software, where labelled ferritin is indirectly identified via these immunogold particles. The success of immunogold labelling can be assessed by conducting negative control experiments and analytical electron microscopy.

This chapter provides an overview and theoretical background of the techniques used in this thesis. A more detailed explanation with precise specifications for the various experiments, devices and software can be found in chapter 5 *Experimental* on page 43.

2.1. Sample preparation

In order to develop a workflow capable of localising ferritin, it is advantageous to choose brain regions with a high ferritin content.

In total we examined three different brain regions for ferritin, two with a high ferritin content and one with less ferritin. These regions are putamen and globus pallidus, nuclei in the midbrain containing H-ferritin¹ in the range of 800 and 1000 $\mu\text{g}/\text{g}$ tissue², respectively and frontal lobe, where the ferritin content is around 450 $\mu\text{g}/\text{g}$ tissue [36]. The location of these brain regions can be seen in Figure 1.2 on page 3.

¹H-ferritin, or the H-chain of ferritin, is the most abundant chain of ferritin in human brain tissue, therefore easier to detect; see also section 1.1.1 *Ferritin is regulating iron levels* on page 2.

²All three weight specifications refer to the tissue in question as wet weight.

Preparation steps overview

Firstly, samples of human brain tissue are obtained from the department of pathology at the Medical University of Graz. Autopsies are done on recently deceased patients, where the brain is removed. Brain regions of interest are extracted and kept in saline solution for the time being, to prevent dehydration, see Figure 2.1a. Brain tissue is quickly chemically fixed in chemicals to stop decomposition and preserve intrinsic structures. To ensure fast and complete penetration of the fixative, the tissue is cut into small, cube shaped pieces. Subsequently, samples are stained with heavy metals, such as osmium and lead, to enhance the contrast of the tissue in the TEM. Finally, samples are infiltrated by a resin which is polymerized under heat. The finished sample is gripped with a specimen holder, which is pictured in Figure 2.1b, and cut into ultra-thin sections of ~ 70 nm on an ultramicrotome, also shown in Figure 2.2a. The sections produced by the ultramicrotome are transferred onto small copper grids, one of which is shown in Figure 2.3b.

These preparation steps are needed to move onto the next phase of the experiment: immunogold labelling, which is described in detail in section 2.2 *Immunogold labelling* on page 11. The following subsections will give a detailed view of every step involved in the sample preparation.

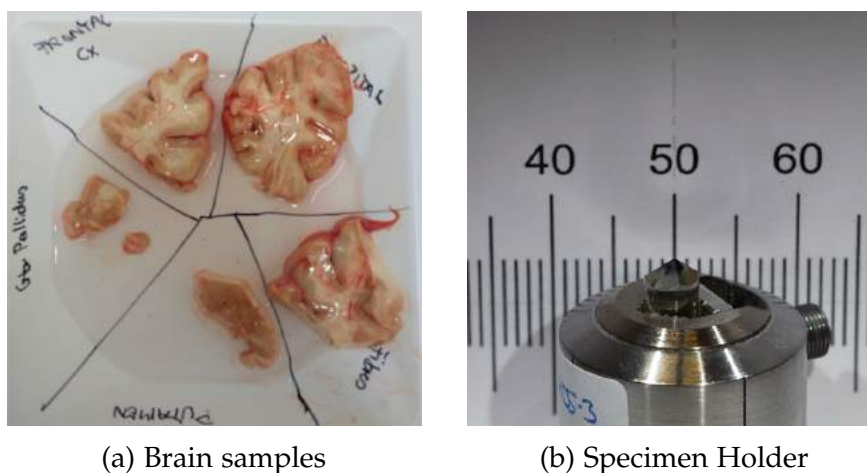


Figure 2.1.: Image **a** shows freshly acquired brain samples from different brain regions, suspended in saline solution. In image **b** a specimen holder is shown, equipped with an LR-white sample of osmated brain tissue. The scale in the background is given in millimetres.

2.1.1. Fixation of samples

The TEM method requires very thin samples, so they are cut into sections of ~ 70 nm. Biological samples are mostly too soft to be cut this thin, especially at room temperature. Furthermore, tissue is degrading rapidly after death and the intrinsic structure is lost quickly [37]. Therefore, samples are chemically fixed using chemicals which link cellular components like proteins or lipids. This process, also called cross-linking, can be imagined as preserving the current state of the cell or tissue; degradation processes come to a halt. The cross-linking of proteins is often

done using chemicals like formaldehyde (FA) or glutaraldehyde (GA) [38]. This allows the sample to be stored for a long time, in buffered solutions³, or better, embedded in resin for use in TEM experiments.

Cross-linking proteins is counterproductive for immunogold labelling

Fixating samples in FA and GA helps to preserve ultrastructure, which is important for properly analysing samples in the TEM. However, too much chemical fixation can be counterproductive for immunogold labelling experiments: cross-linking proteins reduces antigenicity⁴, which is needed for our antibodies to bind to ferritin. A high concentration of fixatives therefore reduces available antigens, which is detrimental for this experiment, since primary antibodies will bind less efficiently. Hence, a reduced amount of fixatives should be used for immunogold labelling experiments. FA might be used in ordinary concentrations of ~2 %, because antibodies are designed to allow FA fixation⁵, but especially GA is known for reducing antigenicity, because it utilizes two aldehyde groups for improved cross-linking of proteins. Therefore, efforts should be made to reduce concentrations of GA as far as ~0.05 % [39].

2.1.2. Enhancing the contrast

After the embedding and subsequent fixation process of the sample, it is undergoing a procedure which enhances the contrast of certain structures. This is achieved using heavy metals or complexes of heavy metals which bind to these structures. In EM, osmium tetroxide (OsO_4) is commonly used as contrast enhancer, which has already been discussed as far back as 1958 [40]. Contrast is achieved due to the high electron scattering rate of heavy metals like osmium in the TEM. Osmium staining works by OsO_4 binding to double bonds in phospholipids, mostly present in cell membranes [41]. The high contrast achieved with this method allows membranes to be easily identified. Furthermore, OsO_4 works as a secondary fixative, because it reacts with carbon-carbon double bonds [42]. These are also mostly present in unsaturated lipids, which are found in cell membranes. This process stabilizes these lipid structures and prevents them from being washed out by solvents.

Osmium was not used for fixation in immunogold experiments for a long time, since it was assumed to reduce antigenicity [43]. However, it has made a comeback in recent years, because of its excellent contrasting properties [44].

$\text{K}_3\text{Co}(\text{CN})_6$ contrast enhancement

Osmium contrasting can be improved by adding $\text{K}_3\text{Fe}(\text{CN})_6$ (potassium ferricyanide), a reducing agent used for improved osmium deposition as far back as

³Long term storage in buffered solutions should be avoided, because some parts of the sample might leach out.

⁴Regions of proteins, in this case the H-chain of ferritin, which are targeted by an antibody, are called antigens. For a better understanding of this process, see section 2.2 *Immunogold labelling* on page 11.

⁵Leitinger, 2018 personal communication

1979 [45]. Since this project is also looking for iron cores of ferritin (see section 2.5 *Analytical electron microscopy* on page 19), $K_3Fe(CN)_6$ is replaced by potassium hexacyanocobaltate ($K_3Co(CN)_6$), a similar reduction agent, which is not containing iron. Due to the similar chemical composition, it is assumed that both $K_3Fe(CN)_6$ and $K_3Co(CN)_6$ react alike.

2.1.3. Embedding of samples

After fixation, samples are significantly harder and structural degradation processes have stopped. However, samples are neither hard enough to be cut by an ultramicrotome, nor do they have the shape to be gripped accordingly. For these reasons, samples are undergoing a process where a resin is used to infiltrate and surround the sample, which is called embedding. Before that, the sample has to be dehydrated, which removes unnecessary water by introducing up to 96 % ethanol to the sample. This step is necessary to remove excess water which interferes with the polymerization process of the resin. The resin is then poured into a casting model, which gives the sample a shape that can be gripped and used for sectioning. The sample is placed inside the casting model, which is then undergoing heat treatment, allowing the resin to polymerize and harden.

LR-white resin for immunogold labelling

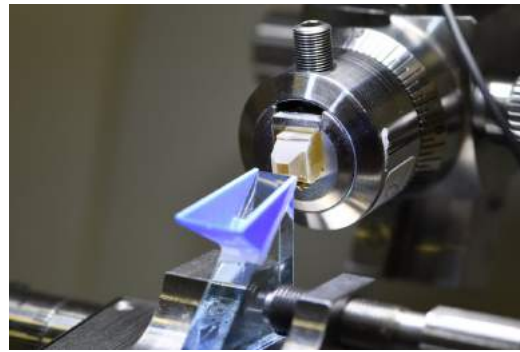
A specialized resin is needed for immunogold labelling experiments. LR-white is often used for this process [46], because its amphiphilic properties [47] enable a more successful antibody-antigen binding rate. This occurs due to enabling antigen-antibody interactions via an aqueous antibody solution, which is applied to the sample, see section 2.2 *Immunogold labelling* on page 11. Hydrophobic resin would prevent this aqueous solution from efficiently interacting with the sample. Another advantage of LR-white is the reduced amount of ethanol which is necessary to dehydrate the sample, accepting the tissue at 70 % ethanol.

2.1.4. Microtome sectioning

Due to the polymerization process, the samples are hard enough to be cut with a sharp glass knife, see Figure 2.2b. Therefore, the sample is placed in a specialized holder and tightly fixed, which is shown in Figure 2.1b. Trimming the edges of the sample ensures a small sectioning window. Afterwards, the sample is placed in the ultramicrotome and ready for the sectioning process. These devices are specialized for ultra-thin sectioning of embedded specimens. They are equipped with an arm in which the sample is attached. This arm describes a vertical movement, causing the sample to glide over a stationary knife. Each turn, a precise feed extends the arm a specific length, generating ultra-thin sections. These sections slide onto a water bath attached behind the blade. This process can be seen in Figure 2.3a.



(a) Ultramicrotome



(b) Glass knife

Figure 2.2.: Image **a** shows a Leica UC7 ultramicrotome, which was used to generate ultra-thin sections. Image **b** shows a glass knife close to a sample, which is mounted in the microtome.

Semi thin sectioning

Firstly, semi thick sections are generated using a glass knife. These sections are needed to find a small area of interest in the sample, since the whole sample is too big to be viewed in the TEM. Localising the desired area is done by transferring freshly cut sections of ~ 250 nm thickness onto glass slides. After removing water from the sections by drying them on a heating plate, they are stained with a 1 % toluidine blue solution which enables the localisation of structures in the sample via light microscopy. If an area of interest has been found, the sample is trimmed to include only the chosen area by means of a sharp razor blade.

Ultra-thin sectioning

The final sample sectioning is done on the same ultramicrotome, but the glass knife is replaced by a much more durable and reliable diamond knife, seen in Figure 2.3a. The sectioning process is very similar to the aforementioned process, but sections are cut to a thickness of only ~ 70 nm. Three to five of these sections are then transferred onto a small copper grid and dried in air, see Figure 2.3b, after being dried with filter paper first. These grids are now ready to be labelled with immunogold.

2.2. Immunogold labelling

Immunogold labelling works by applying a primary antibody to the sample, which specifically binds to the sequence of amino acids present on the H-chain of ferritin. This specific target is chosen, due to an abundance of H-chain ferritin in human brain tissue, see section 1.1.1 *The role of iron storage* on page 2. After applying this primary antibody, a secondary antibody is introduced, targeting the primary antibody⁶. This configuration is represented in Figure 2.4. The secondary

⁶This primary-secondary antibody configuration is mainly used for financial reasons. The production of primary antibodies tagged with a gold particle would be astronomically high. This arrangement allows the production of cheap primary antibodies for almost any protein, that can

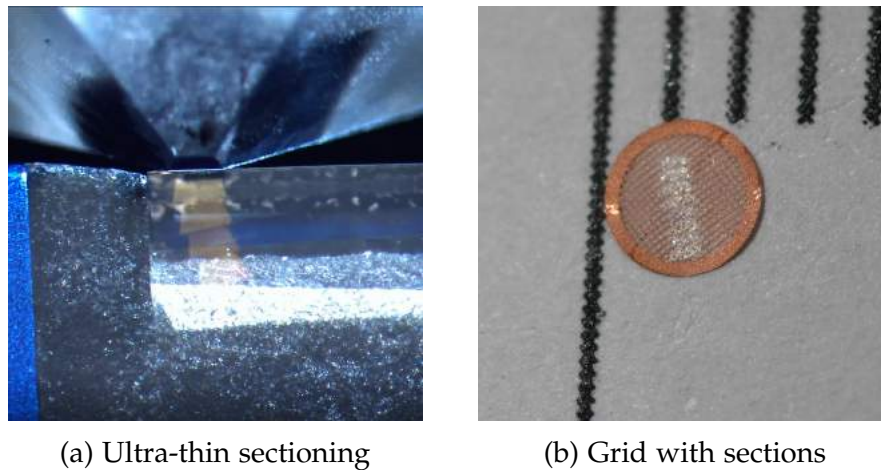


Figure 2.3.: Image **a** shows the ultra-thin sectioning procedure, using a diamond knife. Sections of freshly cut tissue can be seen floating on the surface of the water. These sections are placed on a copper grid, which is shown in image **b**. The vertical scale on top shows a total distance of 5 mm, separated into 1 mm units.

antibody is tagged with a 10 nm gold particle, which is distinguishable from biological tissue, allowing it to be discovered easily in TEM. This way, ferritin can be indirectly localised by identifying gold particles in the sample. Since the antibody-antibody chain generated has a maximum length of around 20 nm, it can be assumed, that ferritin is found close to the gold particle.

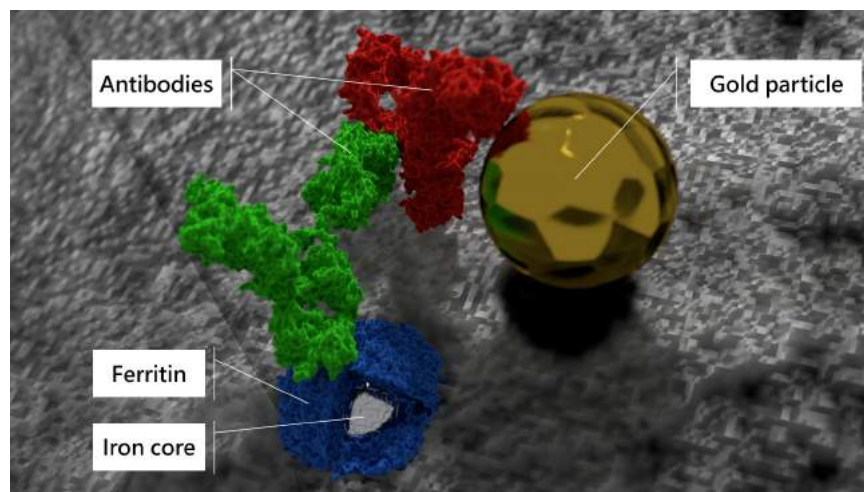


Figure 2.4.: Representation of the immunogold labelling configuration. Ferritin (shown here in blue) is depicted in an open position. On the inside, a 3.5 nm iron core can be seen. The ferritin protein is tagged with a primary antibody (shown in green). A secondary antibody (shown in red) is attached to the primary antibody. It is also covalently linked to a 10 nm gold particle.

be tagged with a non-specialized secondary antibody being capable of targeting many different primary antibodies.

Applying the primary antibody

The process of immunogold labelling is done by placing the grids containing the tissue samples on droplets of the antibody solution, in which the side with the sections is facing the solution. Then the grids are moved from droplet to droplet being incubated with the different antibody and washing solutions. This is depicted in Figure 2.5. The side of the grid carrying the sections of tissue is always facing the droplet.

These droplets start with a solution of phosphate buffered glycine solution (PBG), which is masking charges present on the sections due to their properties, protecting the primary antibody from unspecific binding. The next step involves a blocking solution, which serves the purpose of lowering unspecific binding of the primary antibody and improving the signal to noise ratio⁷. The blocking solution covers most of the surface structures of the tissue and will be replaced by the primary antibody on specific locations, due to the higher affinity of the antibody to its antigen. After blocking unspecific binding sites, this primary antibody is applied.

In this thesis a polyclonal rabbit anti H-chain ferritin antibody was used. Polyclonal means, that the antibody was produced by a random immune reaction to H-chain ferritin. This results in a mixture of antibodies, targeting different epitopes of the ferritin H-chain. An epitope is a part of a protein, to which an antibody can bind. The antibody is applied in different concentrations, to find the best working dilution for this experimental set up. After the antibody has been applied, multiple washing steps are done to remove primary antibodies, which did not bind.

Applying the secondary antibody

After the washing steps, the secondary antibody is applied for approximately half of the primary antibody incubation period. This antibody (host species: goat) binds specifically to the first antibody, targeting epitopes that are present on the rabbit antibody. These epitopes are, of course, not found in human tissue. The concentration of the secondary antibody is usually less than the concentration of the primary antibody. Since a majority of the primary antibody did not bind, less secondary antibody is needed to bind to the primary one.

After extensive washing in phosphate buffered saline (PBS) and double distilled water (ddH₂O), the process of immunogold labelling is finished. Ferritin is now labelled with a gold particle which can be identified in TEM.

2.2.1. Negative controls

Even if the process of immunogold labelling is very well established, errors can occur and result in false positives. To prevent this from happening, the binding specificity of immunogold labelling is checked with negative controls. In this thesis, two different types of negative controls are used. In the first, the primary antibody is left out on purpose, in the second one, the primary antibody is interchanged by

⁷The signal to noise ration describes the amount of gold particles actually bound to ferritin, compared to those bound to any other structure in the sample.

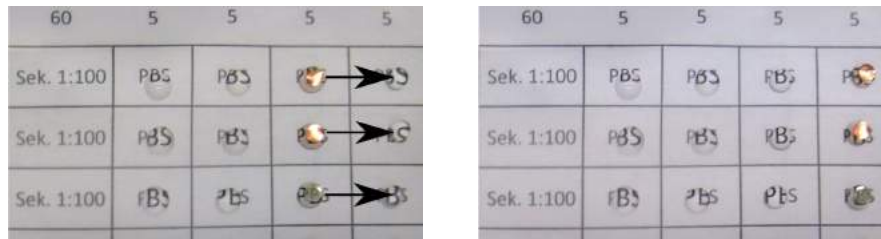


Figure 2.5.: These two images show how grids are placed onto droplets of PBS solution and how they are moved from droplet to droplet. The droplets are placed on parafilm, below which a text can be seen, displaying which solution is present. Arrows indicate the direction in which the grids are moved. The numbers on the top indicate the time in minutes that the grids incubate at any given location.

a different primary antibody from the same immunoglobulin family, hence called isotype, targeting structures not found in human brain tissue.

Negative control by absence of a primary antibody

In this type of negative control the primary antibody is interchanged by a regular PBG solution. In this configuration, the secondary antibody should not be able to bind to the sample. In the TEM, only a few gold particles should be seen, which can be characterized as gold background, assessing the signal to noise ratio. This background signal is subtracted from regular sample measurements to ensure that the number of gold particles comes mainly from positive binding of the primary antibody.

Isotype control by changing the primary antibody

The isotype negative control evaluates if the primary antibody is binding unspecifically to structures that do not belong to the protein of interest. This is done by interchanging the primary antibody with an antibodies from the same immunoglobulin family and host species. The secondary antibody can still bind to these antibodies, but they should not be able to bind to antigens present on the sample. If only a normal gold background signal is found in images acquired in the TEM, the isotype control can be seen as successful.

Samples are now ready for observation in a TEM. However, the contrast produced by OsO_4 is not enough to reliably describe structures in the sample and to identify cells. Therefore, further contrasting is done, introducing even more heavy metals to the tissue.

2.2.2. Contrasting

Contrasting, serves the purpose of further increasing the contrast of the tissue by extensive electron scattering using heavy elements. For a better understanding of this process in TEM, see section 2.3 *Transmission electron microscopy* on page 16. Elements such as lead and platinum are often used for this. They induce strong scattering of incoming electrons, which is not the case for the carbon rich

biological tissue. This way, a better contrast is generated and structures are more distinguishable.

In this thesis, both, a strong and a weak contrasting approach was taken. In heavily contrasted samples, structures are more easily distinguishable and cells can be better identified. However, due to the decreased difference in contrast between tissue loaded with heavy metals and the gold particles that are introduced in immunogold staining to indicate ferritin, it is harder to locate these gold particles. This is especially true for computer systems, which try to automatically identify and count these gold particles.

In order to be able to identify these gold particles automatically, a second approach, where tissue was stained only with a minimum amount of heavy metals, was introduced. Algorithms are able to identify gold particles more reliable in this mildly stained tissue. How these algorithms identify gold particles is elaborated in section 3.4.2 *Image analysis of mildly stained tissue* on page 30.

Heavily stained tissue

Both staining approaches used the same kind of tissue, but the samples for this heavy staining approach were already infused with more OsO_4 to begin with, see also subsection 2.1.2 *Enhancing the contrast* on page 9. Contrasting of the tissue is done after immunogold labelling on grids. These grids are inserted into a device which performs an automated staining procedure. This staining instrument performs several washing steps, before infusing the tissue with two different types of heavy metals. First, Pb-citrate is applied, the chemical structure of which can be seen in Figure 2.6a. This chemical further enhances the contrast provided from osmium, by interacting with regions where osmium is already present, as well as other regions, such as ribosomes and cytoskeletons [48].

Platinum blue, the second chemical which is applied, is often used as a replacement for uranyl acetate, a well documented, but radioactive contrast enhancing agent [49]. The chemical structure of platinum blue can be seen in Figure 2.6b.

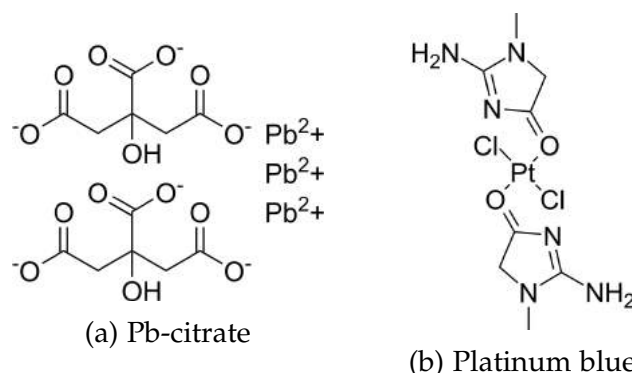


Figure 2.6.: Image a shows the chemical structure of the contrasting agent Pb-citrate, usually applied to the tissue in a 3% w/v aqueous solution. Image b shows the chemical structure of Pt-blue, also a contrast enhancing agent.

Mildly stained tissue

In order to keep the amount of contrast in the tissue at a low level, only a minimal amount of Pb-citrate is applied to the sample. This approach makes it easier to identify gold particles in the tissue, it is however more difficult to identify structures and cells. Contrasting was done by hand using a pre mixed solution from a dispenser. From the solution only a droplet is put onto parafilm, the whole set-up being enclosed in a watch glass. In the same fashion as mentioned before in section 2.2 *Applying the secondary antibody* on page 13, the grid is placed onto the droplet and incubated for a specific amount of time. Since Pb-citrate is precipitating in presence of CO₂, special caution is needed to keep exhaled air from the droplet. The precipitation of Pb-citrate leads to water insoluble lead carbonate (PbCO₃) contaminations on the sample [48]. This process can partly be avoided by placing beads of NaOH close to the Pb-citrate droplets in order to suppress this reaction by raising the pH value of the surrounding.

The samples are finally ready to be viewed in the TEM. The next chapter will give a short overview how EM works and which experiments can be done with this type of microscope.

2.3. Transmission electron microscopy

The basic principle of an electron microscope (EM) is very similar to an optical microscope. The most striking difference is however, that the resolution of light microscopy is limited by the wavelength of visible light. This boundary is set at around 200 nm for the best microscopes available today. Achieving a higher resolution than that can only be done utilizing complex workarounds [50]. Since we are detecting ferritin by labelling it with a 10 nm gold particle, the microscope should have a resolution of at least 5 nm or lower. This can be achieved using a transmission electron microscope (TEM). The microscopes used in this thesis, a Zeiss EM 900 and a FEI Tecnai G2 20 are easily capable of detecting structures this small and much smaller.

2.3.1. Transmission electron microscopy basics

An image of the basic configuration of a TEM can be seen in Figure 2.7 and will be used in explanations in the following section. Close to the top of the microscope, electron emission is taking place when a LaB₆ (lanthanum hexaboride) cathode (A) is heated to ~2000 K while a strong voltage is applied between the cathode and the copper anode (B). Electrons accelerating towards the anode are focused to a beam by the Wehnelt cylinder, directly below the cathode. Coils (C, D) are used to form the beam, while coils (I) focuses the beam after it passes through the sample, controlling the magnification of the beam. Coils (J) control the size of the beam that reaches the screen (K). The strongly scattered electrons are removed by an aperture (D), before reaching the sample, thus creating contrast.

The copper or nickel grids containing the sections are mounted in a grid holder (F), which is inserted into the microscope via an air lock. This air lock is protecting the vacuum inside the microscope. A device called stage is mounted perpendicular

to the microscope and moved by multiphase motors in a very precise fashion. Inserting the grid holder into the stage and through the air lock places the grid in a perpendicular position to the electron beam, which is shown in Figure 2.7b. Changing the position of the stage also changes the position of the grid in the electron beam. This way, the specimen can be observed at different locations.

After passing through the sample, the beam can be observed on the fluorescent screen (**K**) on the bottom of the microscope, also seen Figure 2.7c from a front view of the microscope. When the screen is lifted, a bottom mount camera can be inserted, which is exposed to the electron beam and images are generated using a charge-coupled device (CCD) chip that is perpendicular to the beam, see Figure 2.7d. This camera is used to generate images of the sample at various magnifications.

2.3.2. Transmission electron microscopy operation

In order to generate enough information to assess the number of gold particles which label ferritin, large areas of samples have to be viewed. Since these gold particles are only 10 nm in size, it is crucial to choose a magnification that is both able to detect these gold particles reliably, but also views an area large enough to detect enough gold particles in a reasonable amount of time.

Large areas can be acquired by stitching together several smaller images to create an image of considerable size. This process also allows to get an overview of the general state of the sample, regarding tissue quality and the distribution of gold particles. Stitching can be done manually or by utilizing a software which is capable of stitching together images at a high magnification. Stitched images, also called montages or maps, can later be analysed, either by hand or automatically.

2.4. Image Analysis

Images generated by TEM are analysed with a specialized image analysis software called *FIJI is just ImageJ (FIJI)* [51]. This open source software provides image analysis and image manipulation features.

After loading the desired 16-bit image into the console, a threshold is generated blocking out all grey values of the image above a certain range, resulting in an 8-bit image, where the gold particles and a few other, irregular shaped impurities are black, light grey being the rest of the image. Using a particle analyser, gold particles, which have a well defined shape and size, can easily be counted. This is done by including only particles with a narrowly defined size, shape and other features, see section 4.2.2 *Improving the automatic detection of gold particles* on page 39. *FIJI* analyses and counts these particles and overlays them with a mask, so that they can be manually checked and verified.

Counting and analysing the distribution of these gold particles might be a safe way to identify ferritin proteins in human brain tissue. The use of negative and isotype controls certainly confirms the validity of this workflow. However, this process is detecting gold particles, which are assumed to be bound to ferritin.

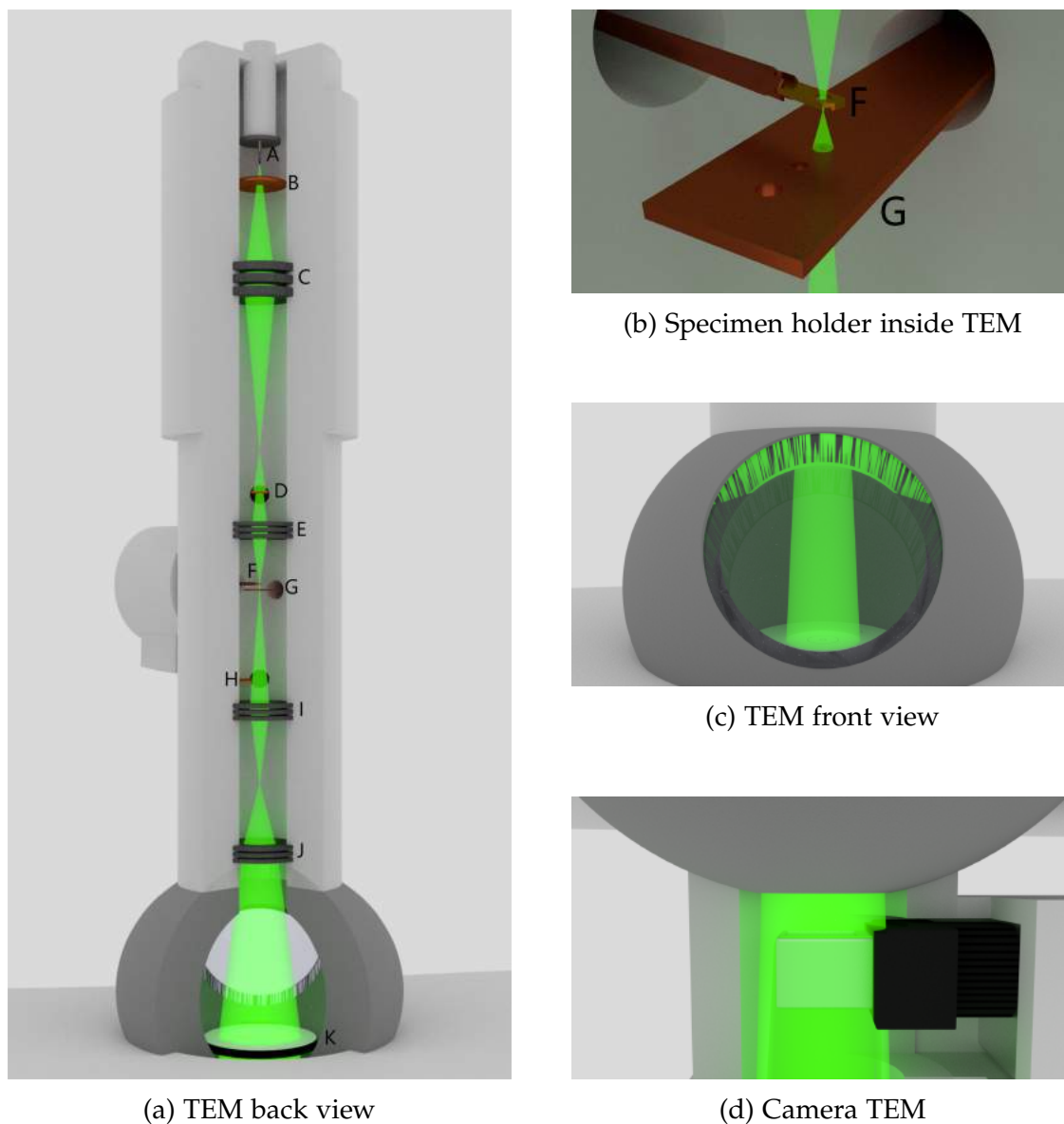


Figure 2.7.: Scheme of a transmission electron microscope. Image **a** shows an opened back view of the body of a TEM. An electron beam is generated from a LaB_6 cathode (**A**). Electrons are accelerated in the direction of the anode (**B**). The beam is condensed on a condenser lens (**C**). After passing through the condenser aperture (**D**), the beam is once more condensed by the objective lens (**E**), before passing through the sample (**F**). A close up look of this configuration can be seen in image **b**. The beam is further reduced by the objective aperture (**G**), before being condensed by the diffraction lens (**I**) and the projector lens (**J**). The selective area aperture is only used for special applications. In image **c** the front view of the TEM with a lowered screen can be seen. Image **d** shows the electron beam projecting an image onto the bottom mounted CCD camera. For this, the screen seen in image **c** has to be lifted.

Another way to certify this workflow, to legitimise that the detected gold particles are indeed labelling ferritin, is the use of analytical electron microscopy.

2.5. Analytical electron microscopy

TEM offers a variety of methods to analyse the chemical composition of samples. In this thesis, these techniques are used to assess the validity of immunogold labelling. To increase the degree of certainty of the obtained results regarding the actual binding of gold particles to ferritin, their elemental composition has to be investigated. In order to determine the elemental composition of certain areas in a sample, specialized electron microscopic techniques are used. These techniques are based on the intrinsic property of atoms in the sample which lower the energy of passing electrons or emit X-rays at characteristic wavelengths after encountering passing electrons.

2.5.1. Analytical electron microscopy basics

The electron beam interacts with both the atomic nuclei and the electrons in the sample. Certain interactions cause an energy loss in the beam. This energy loss is specific for the chemical element and the shell of the electron that the beam interacts with[52]. This effect is used when detecting the chemical nature of the specimen with an energy filter (electron energy loss spectroscopy, EELS, and energy filtered transmission electron microscopy, EFTEM). These will be described in more detail in the next section.

Not only energy absorption, but also energy emission differs between elements. When energy from a passing electron is absorbed by an atom, electrons orbiting the atomic core are able to occupy states of higher energy. However, these higher energy states are unstable and can only be occupied for a very short amount of time before falling back into the ground state. Upon falling back, these electrons emit photons of various wavelengths, including X-rays, of a characteristic wavelength as a way to release this excess amount of energy [53]. The wavelength of the emitted X-rays differs between elements, which can be used in another spectroscopic method named energy dispersive X-ray analysis (EDX), which is elaborated in more detail in subsection 2.5.3.

2.5.2. Energy Filtered Transmission Electron Microscopy

After the electron beam has passed through the sample, these electrons have different energy levels when they reach the CCD camera. The amount of energy that the beam loses is specific for the chemical element it interacted with. Therefore differences in beam energy can be utilized to obtain images showing different chemical elements in the specimen at nanometre resolution.

In an energy filter (prism), several magnetic fields deflect the beam at an angle of approximately 90° and split up the different energy levels of the beam, see Figure 2.8a. Faster moving electron end up vertically lower than slower electrons,

due to their shorter time period in the magnetic field and therefore the resulting lesser deflection of their path through it.

Before converging the beam and focussing all these separated electrons on the detector again, which can be seen in Figure 2.8b, an energy slit is introduced. This slit can effectively block out all electrons above and below a certain energy range, because electrons travelling at different kinetic energies (or speeds) also differ in wavelength. Inserting the slit, which is shown in Figure 2.8c, causes only the electrons with a chosen energy range (or wavelength) to reach the CCD camera. If the slit only allows an energy range characteristic for iron to reach the camera, an image is generated that only shows the iron atoms in the sample, at nanometre resolution. [54] This method is used to produce elemental maps, which can be used to locate iron, gold or any other element which is looked for.

In this thesis, an elemental map for iron is generated by using the three window method. In short, one image is acquired, where the energy slit is adjusted to receive signal above the characteristic energy range for the element of interest (e.g. for iron this energy range is 54 eV). Subsequently, two more images are acquired, where the energy slit is set to measure a signal below that energy range. These two images can now be subtracted from the original image, producing an elemental map.

Drawbacks of EFTEM include the limitation to a smaller image size, compared to conventional TEM, if small particles should be analysed in a reasonable amount of time. Only a small portion of electrons, which reach the CCD camera are energy loss electrons, actively contributing to the filtered image, therefore long exposure times are needed to acquire images in EFTEM.

2.5.3. Energy dispersive X-Ray analysis (EDX)

As described in subsection 2.5.1 *Analytical electron microscopy basics* on page 19, atoms can emit photons (X-rays) after interacting with high energy electrons, see the blue emission in Figure 2.8d. In order to know where in the sample these X-rays came from, the electron beam has to focus on a very small area. This is possible with a special mode of TEM called scanning transmission electron microscopy (STEM), in which the image is produced by repeatedly moving a very small beam over the sample.

Scanning transmission electron microscopy

Focusing the electron beam on a very small area in the sample makes it possible to correlate the position of the electron beam with the appearance of X-rays. A ring shaped detector placed below the sample is able to assess the weight of the atomic nuclei that are present in the line of the focused beam, an image of which can be seen in Figure 2.8d (E). This detection is made possible by the fact that heavy nuclei like gold or lead deflect electrons to a much higher degree than lighter elements. This high angle annular dark field (HAADF) detector can therefore only distinguish between light and heavy elements.

By moving this focused beam in a precise scanning fashion, each location that has been passed by the beam can be assigned a darkness value, creating an image from a compilation of different darkness values at different locations. This

scanning mode also allows to assign each location with a spectrum of X-ray values, hence scanning small areas allows collecting information about the elemental composition of this area.

Detecting X-Rays

X-rays are emitted in every spatial direction when atoms are interacting with high energy electrons. Tilting the sample in the direction of a detector between 10° and 15° [55] allows an increase in X-ray yield, because (i) the sample is not perfectly flat and signal might get lost in grooves, and (ii), the penetration depth increases with a tilted sample, producing more X-rays, thus more signal. A typical detector is made of a silicon crystal doped with lithium, also called Si(Li). This crystal absorbs incoming X-rays, generating a number of electron-hole pairs, which is proportional to the wavelength of the X-ray. After being amplified, these electron-hole pairs can be counted, revealing the wavelength of the incoming photon. To keep a good signal to noise ratio, the detector has to be cooled with liquid nitrogen, supplied from a dewar, seen in Figure 2.8a (G). This process can be repeated up to 20.000 times per second, generating a spectrum in a chosen energy range. These generated spectra reveal the elemental composition of the analysed area.

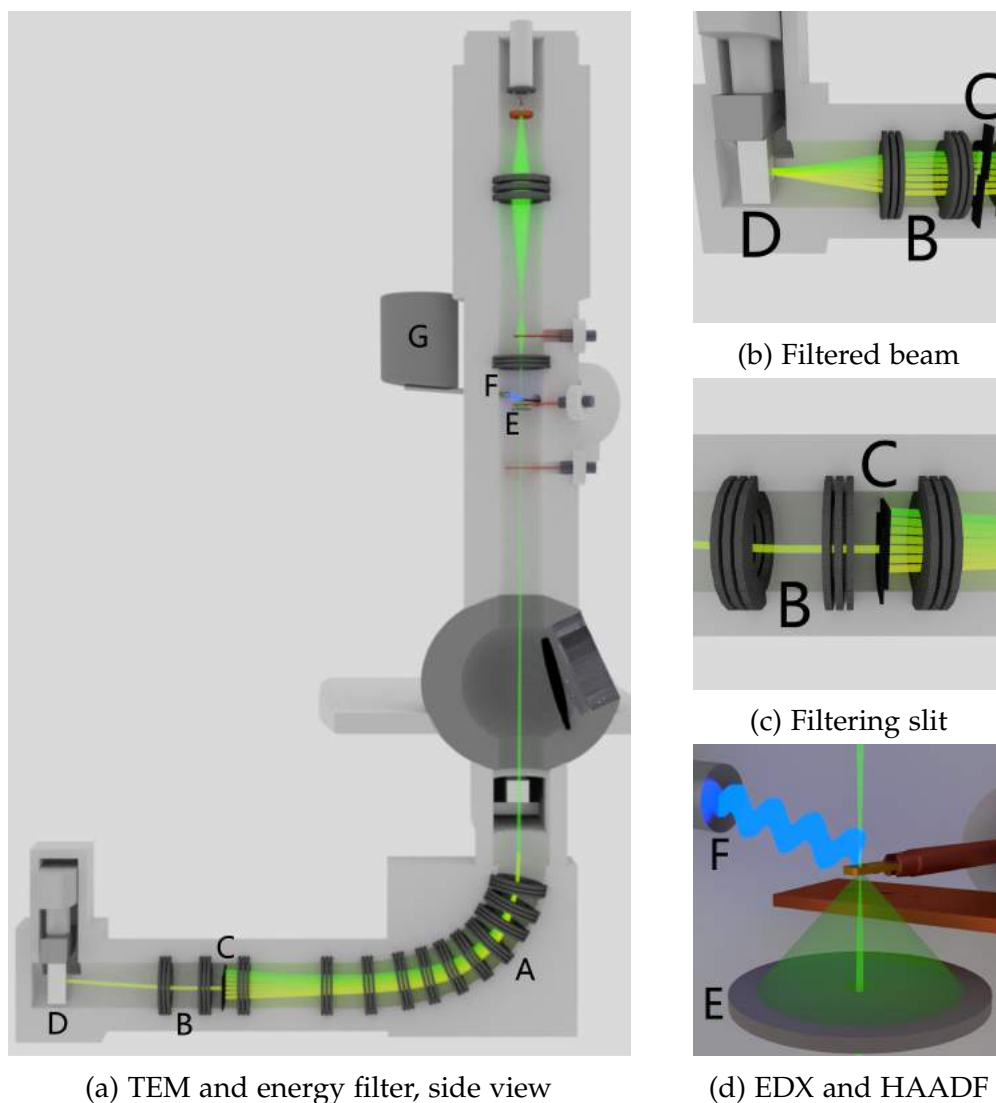


Figure 2.8.: Image **a** shows an opened side view of a TEM with an energy filter (**A**). Here, the beam is deflected and split up into different energy levels. At the energy filtering slit (**C**), a close up can be seen in image **c**, some of the beam is blocked. This enables filtering for specific energy values. In image **b** a unfiltered beam can be seen. Quadrupole and hexapole lenses (**B**) are responsible for beam guidance, after that, the energy filtered image is projected onto the camera (**D**). In the upper part of the microscope, see image **d**, an HAADF detector (**E**) is responsible for image acquisition during EDX measurements. The EDX detector (**F**) is attached to a cooling dewar (**G**), filled with liquid nitrogen and mounted outside the microscope.

3. Results

Immunogold labelling with a primary antibody directed against ferritin heavy chains, allowed the detection of ferritin within tissue samples taken from human brain. Two separate sets of experiments were made, one for cell-specific localisation of ferritin, and the other set for tissue specific localisation of ferritin. For cell specific ferritin detection, a heavily contrasted sample was preferred, because it enabled recognising cell types. Tissue specific localisation of ferritin was best done on mildly contrasted samples, which allowed an automated detection of immunogold particles. The quality of the experiment was elaborated with negative controls, which assessed the selectiveness of the antibody, as well as analytical EM, analysing if gold particles and ferritin iron cores were found in close proximity to each other.

Firstly, a suitable fixation and embedding workflow for human brain tissue had to be found. After that, the process of immunogold labelling and the subsequent contrasting of the tissue was refined. Thereafter, the acquisition of images in TEM and the analysis of these images was done. Finally, these result were validated using analytical EM. The following sections give detailed information on how this workflow was established and which parameters worked best for the goal of localising and quantifying ferritin in human brain tissue.

3.1. Fixation and embedding refinement

Efforts were made to refine fixation and embedding procedures to establish the optimal practice for brain tissue. This process had to ensure that the tissue is properly chemically fixed, while enabling the presence of available ferritin antigens for immunogold labelling. Different methods of fixation and embedding techniques have been tested and compared to each other.

3.1.1. Optimal fixation procedure

The fixation of brain tissue was done in an aqueous solution, containing 2 % formaldehyde (FA) and 0.1 % glutaraldehyde (GA). The tissue was incubated in this solution for three hours, after which the solution was replaced by a Na-phosphate buffer. Minuscule amounts of sodium azide (NaN_3) were added to suppress fungal growth [56]. After this procedure, the tissue was firm enough to be manipulated with ceramic tweezers, and the internal structure was preserved reasonably well. Storage of the samples was done in a fridge at 4 °C in Na-phosphate buffer.

This FA concentration is quite common for immunogold labelling, hence this concentration was not changed in different experiments. Minimal GA concentrations were used to provide at least a second fixative, targeting different structures than FA regarding cross-linking. A higher concentration of GA was avoided, due

to the well reported negative effects of GA on antigenicity [57]. A third fixative, piperazine-*N,N'*-bis(2-ethanesulfonic acid) (PIPES) was tested for its ability to stabilize lipids.

The use of PIPES buffer for lipid stabilisation

An improvement for the fixation method would have been the stabilization of lipids in the sample, because brain tissue contains a high amount of lipids. PIPES buffer has been described to be highly beneficial for lipid preservation in biological tissue [58]. However, trials with PIPES buffer fixation (4% PIPES, 2% FA) from a protocol by Skepper J. [59] performed worse in terms of antigenicity: samples chemically fixed with PIPES buffer showed a gold background of $\sim 40\%$, which is much higher than the gold background from conventional fixation (compare Table 3.1). Even though an improvement in the stabilisation of lipids inside axons can be seen (for this, compare Figure 3.1 with Figure 3.1c), the high gold background renders this benefit useless.

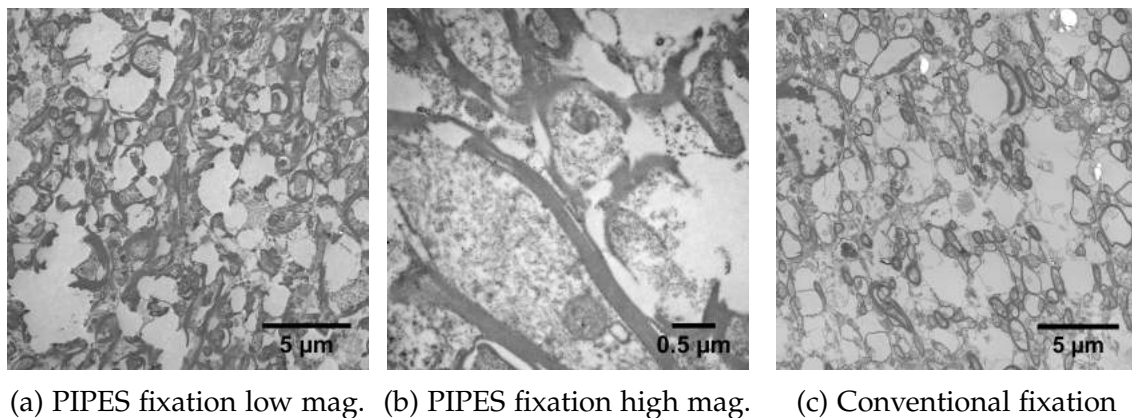


Figure 3.1.: Human brain tissue chemically fixed with 4% PIPES and 2% FA embedded in LR-white. Stained with Pb-citrate for 15 min and Pt-blue for 7 min. Picture **a** shows a low magnification of the tissue; overall structure is adequately preserved. Big parts of the tissue are bloated or ripped apart, which might be due to the rapid decomposition of brain tissue after death. Picture **b** shows a higher magnification of picture **a** in the upper left corner. The inside of axons seems to be better preserved than comparable tissue chemically fixed without PIPES buffer. Image **c** shows a reference image, which was not chemically fixed with PIPES.

Osmium fixation and contrast enhancement

Osmium has been reported to act as a secondary fixation agent, as well as a contrast enhancer. Trials with different osmium concentrations were done to assess the influence of osmium on contrast enhancement and tissue fixation. In order to estimate how these properties change with lower concentrations of osmium, an aqueous solution of 0.4%, 0.1% and 0.01% OsO_4 was tested. Since samples for cell identification do not benefit from a reduced amount of osmium, because strong contrast in the tissue is desired, this test was solely done to see how far osmium concentrations can be reduced to improve the conditions for automated gold

identification, while still profiting from the positive properties of OsO_4 . An image with a conventional amount of osmium (1 % OsO_4) can be seen in Figure 3.1c.

Osmium fixation with 0.1 % OsO_4 with an incubation time of two hours gave ideal properties for automated gold counting, see Figure 3.2b. These low osmium concentrations allow slightly contrasted tissue, still benefiting from the fixing properties of osmium. This low contrast makes it easier for automated systems to identify gold particles.

Fixing with 0.4 % OsO_4 did neither result in a better fixation, nor did it improve the contrast of the tissue significantly. Differences in contrast using lower OsO_4 concentrations can be seen in Figure 3.2. The structural integrity of the tissue did not differ significantly between 0.1 % and 0.4 % OsO_4 . This could mean that the fixing properties of OsO_4 are already working at low concentrations. Fixing with 0.01 % OsO_4 produces samples with washed-out structures, making it difficult to find a proper focus.

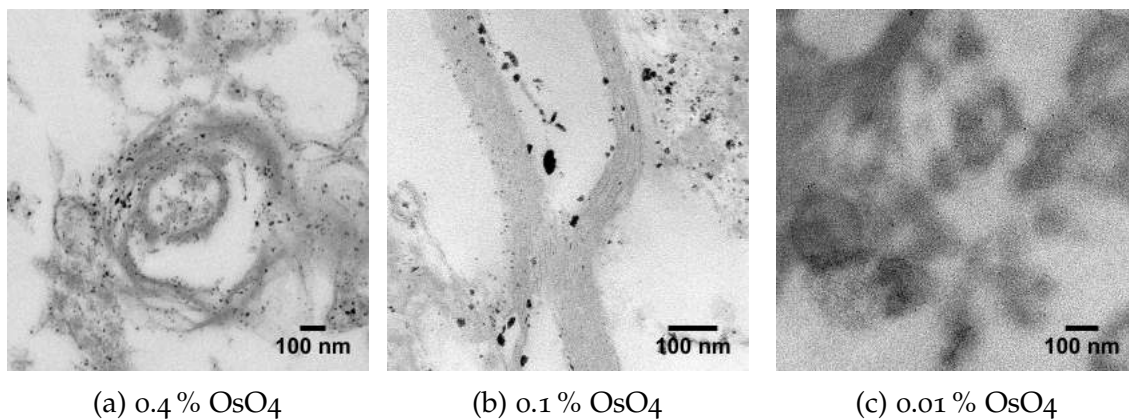


Figure 3.2.: Differences in contrast, when using various OsO_4 concentrations. All samples are of putamen tissue chemically fixed in 2 % FA and 0.1 % GA embedded in LR-white with no further contrast enhancers applied. Apparent contrast differences can be seen between 0.1 % OsO_4 and 0.01 % OsO_4 . Only minor differences in contrast can be seen between 0.4 % OsO_4 and 0.1 % OsO_4 . Black dots in pictures **a-b** are agglomerations of OsO_4 .

3.1.2. LR-white embedding refinements

Tissue was embedded in LR-white resin to enable sufficient interaction between antigens and antibodies. Several attempts of improving this process have been made, including the use of 100 % ethanol (EtOH) for dehydration, and the exclusion of oxygen under reduced pressure.

Using absolute ethanol for dehydration

The dehydration of tissue before embedding serves the purpose of removing water from cells, which would be disadvantageous for the subsequent polymerization process of the resin¹ The distributor of LR-white suggests the use of 70 %

¹Areas of non-polymerized resin can be a real problem in TEM, especially with LR-white. These areas are prone to break during electron exposure, destroying parts of the sample.

EtOH for dehydration. We wanted to see if the use of 80 and 100 % EtOH improves the quality and stability of the tissue. Both attempts can be seen in Figure 3.3.

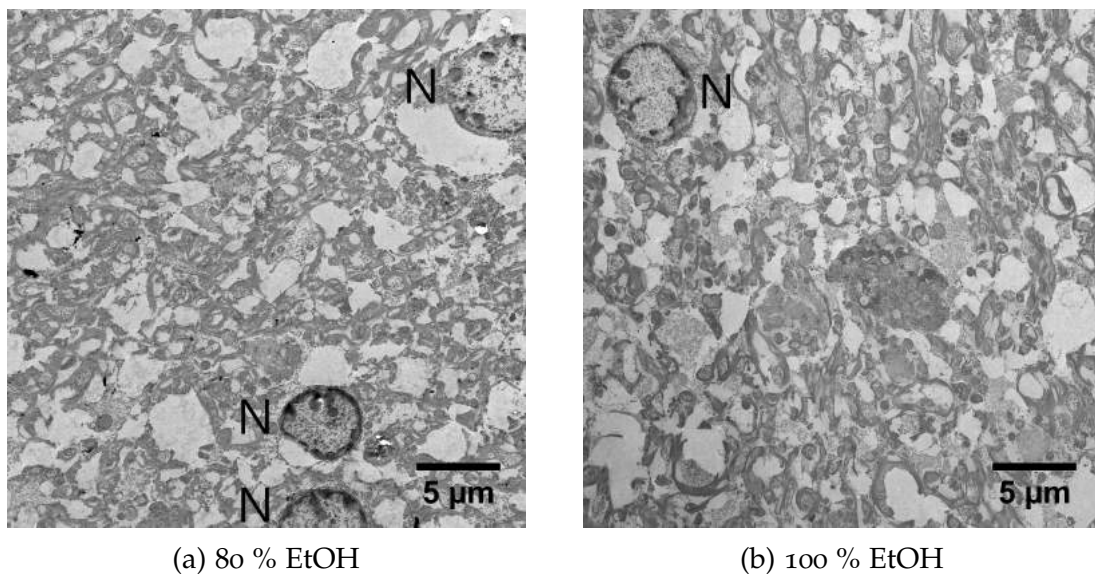


Figure 3.3.: Image **a** and **b** show human brain tissue (putamen) dehydrated with 80 % and 100 % EtOH. Little difference can be seen in the quality, or the number of holes in the tissue. The black letter N marks nuclei, which are well preserved and visible in both images.

However, none of these attempts could be considered successful, because neither improved the quality of the tissue, nor increased the stability of the sample. The suggested use of 70 % EtOH by the distributor of LR-white was utilised and showed satisfactory results.

Excluding oxygen for polymerization by applying vacuum

LR-white needs the exclusion of oxygen for proper polymerization at high temperature. Routinely, liquid LR-white is filled in gelatine capsules and sealed airtight, however, some air always remains trapped inside. To counteract this circumstance, samples were left open during heat treatment, whilst a reduced pressure of ~20 mbar was applied.

During polymerization, LR-white evaporated under reduced pressure, less than half of the original amount was found at the end of the polymerization process. Even a slow reduction of pressure, lowering the pressure 100 mbar per hour during heat treatment, until 20 mbar were reached, did not reduce LR-white evaporation significantly. Hence, this approach to improve polymerization process was no longer used.

3.2. Immunogold labelling

To establish a proper protocol for immunogold labelling in human brain tissue, the optimal dilution of the primary antibody had to be found. Tests were done with different concentrations, as well as two different suppliers for this antibody.

The secondary antibody was kept at a constant dilution to reduce the complexity of this experiment.

Negative controls assessed the labelling quality of every sample, to estimate the amount of gold background. Since many protocols suggest the use of nickel grids instead of copper grids, additionally, some samples were labelled on nickel grids. This test was done to check, if the material has any influence on immunogold labelling quality and/or resistance against corrosion.

3.2.1. Primary antibody results

Dilutions for primary antibodies ranging from 1:10 up to 1:500 are quite common for immunogold labelling. The tests performed in this thesis were done with dilutions of 1:50 and 1:100, because dilutions in this range were tested beforehand and gave sufficient results.

Tissue cut at ~ 70 nm was labelled with a 1:50 and 1:100 dilution of anti ferritin H-chain antibody. In addition, two different suppliers for this antibody were tested, namely *Bioss* and *Abcam*. The secondary antibody was kept steady at a 1:100 dilution. Tests were performed on two different brains in the frontal white matter (FWM), where areas in the sample were randomly selected.

The highest amount of labelled ferritin was achieved with a 1:50 dilution of *Bioss* primary antibody, see Figure 3.4. *Abcam* primary antibodies performed significantly worse with the same dilution. A 1:50 dilution of primary antibody showed considerably better tagging results than a 1:100 dilution.

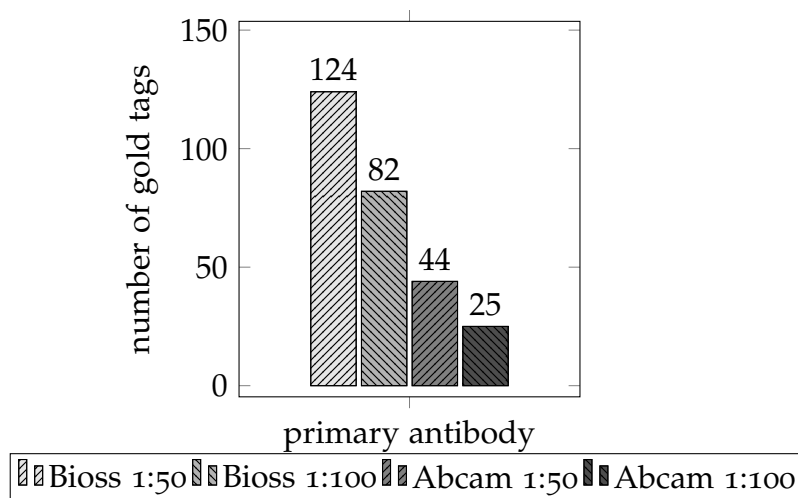


Figure 3.4.: Testing primary antibodies for their labelling quality. Primary antibody rabbit anti-ferritin H-chain from different producers (*Bioss*, *Abcam*) and different dilutions (1:50, 1:100) was tested. A secondary antibody (goat anti-rabbit), tagged with a 10 nm gold particle, was applied in a 1:100 dilution to all samples. The height of the graph shows the number of gold particles per $100 \mu\text{m}^2$ of sample.

3.2.2. Negative controls

Negative controls were conducted by omitting the primary antibody, therefore leaving no antigens for the secondary antibody to bind to. This procedure revealed

a low gold background for *Bioss* antibodies (1:50 dilution), but a high background for *Abcam* antibodies, see Table 3.1. The gold background refers to the unspecific labelling of tissue by the secondary antibody. It is calculated by comparing the labelling rate of regularly labelled tissue to negative controls.

Isotype controls

Isotype controls were conducted by exchanging the primary antibody with normal rabbit IgG. This antibody does not target antigens present in human tissue, hence the measured gold background should be approximately the same as in regular negative controls.

The gold background was measured to be 5% for a dilution of 1:1000 IgG isotype, similar to regular negative controls. This low gold background supports the assumption that most of the signal in regular immunogold labelling specific, i.e. resulting of the primary antibody binding to ferritin.

Table 3.1.: Gold background on samples used for cell identification. The gold background is determined by the quotient of gold particles counted in $100 \mu\text{m}^2$ of negative control tissue, divided by the number of gold particles counted on $100 \mu\text{m}^2$ of regularly labelled tissue.

Antibody	Dilution	Gold background [%]
Bioss	1:50	5
Bioss	1:100	8
Abcam	1:50	15
Abcam	1:100	27

3.3. Contrasting

After the labelling procedure was completed, the samples were either stained heavily with Pb-citrate for 15 min and platinum-blue for 7 min, or stained mildly with only Pb-citrate for 30 s.

3.3.1. Heavily stained tissue results

The use of large amounts of heavy metals for staining resulted in highly contrasted tissue, which should allow cell identification. Immunogold identification was performed manually, see Figure 3.5. Gold particles could easily be counted by hand, due to their round shape and evenly distributed size of ~ 10 nm.

The identification of cells did prove to be difficult, due to the quality of the tissue, suffering heavily from autolysis. However, certain cell types were less affected by autolysis effects and could thus be identified. Most axons, for example, could easily be recognized by the surrounding myelin sheath. A cell specific ferritin count in those cell types that are identifiable is possible but was beyond the scope of this thesis.

3.3.2. Mildly stained tissue results

Samples for automated immunogold counting were only lightly stained by hand, using Pb-citrate for 30 s. This process enables a sufficient difference in contrast between gold particles and the surrounding tissue, allowing for automated gold identification in tissue. The whole procedure for automated gold particle identification can be seen in Figure 3.7. Mildly stained tissue did not provide enough contrast to identify any cells in these samples.

3.4. TEM image acquisition

Samples of heavily stained tissue were analysed on a Zeiss EM-900 80 kV TEM, while mildly stained tissue was inspected using a FEI Tecnai G2 20 200 kV TEM. The switch between those two microscopes occurred, because the availability of both was not always given.

3.4.1. Acquiring images of heavily stained tissue

The acquisition of images for heavily stained tissue was done on the EM-900 at 80 kV with a magnification of 20.000x. The high magnification was necessary to reliably identify gold particles in the heavily stained tissue. These small images were stitched together to create a bigger map, which was used to get an overview of the tissue. Stitching was done automatically with a code created for the stitching function in *FIJI*, feeding images into the software and stitching them accordingly. This code and an explanation for the code can be seen in section B.1 *Code* on page 51. These stitched images are the size of 4x4, or 16 images; this image size of 64 μm^2 proved to be sufficient to identify cells and ferritin, while keeping a reasonable file size. The analysis of these images and the counting of gold particles was done by hand using the *Multi Point Tool* provided in *FIJI*. An image where both stitching and gold particle identification was applied, can be seen in Figure 3.5.

3.4.2. Acquiring images of mildly stained tissue

Mildly stained samples were analysed on the Tecnai G2 20 at a voltage of 120 kV. This microscope was equipped with the freeware *SerialEM*, which is specifically designed to automate certain processes of a TEM. Other than the manual acquisition of images for heavily stained tissue, *SerialEM* provides an automated tool for generating larger images by stitching together smaller, high magnification images, thus generating a map².

Maps were generated by stitching together 90 images at a magnification of 11.500x, hereby creating a map the size of $\sim 100 \mu\text{m}^2$. This image size was chosen, because the map function does not produce maps larger than 90 images. A map size larger than that value will disable the function of stitching these images at a

²The Zeiss EM-900 did have a function for generating maps, however, its software was neither calibrated to acquire images at 20.000x, nor did it result in stitched images of acceptable quality, even at lower magnifications.

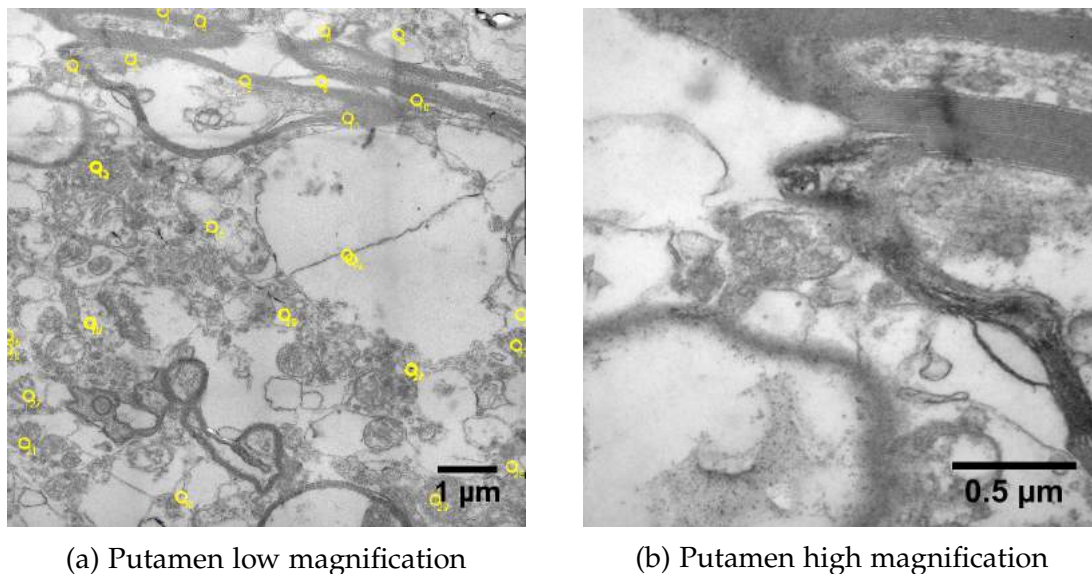


Figure 3.5.: Stitched image of heavily stained putamen tissue. Gold particles were labelled by hand. Yellow circles indicate gold particles which label ferritin. Image **a** shows an overview of $64 \mu\text{m}^2$, while image **b** shows a close up of the top left corner.

high quality. Once a map size has been chosen by outlining the desired map at a lower magnification (e.g. 1.700x) and the parameters for the map acquisition have been set, other locations can be acquired with the same settings. This is simply done by marking the desired location, where the marker serves as the middle point of the new map. A map generated from frontal white matter (FWM) can be seen in Figure 3.6. In this map, the localisation of gold particles was already done. The automated identification of gold particles is explained in the next section, in this image, the gold particles were marked with a white box and a black index.

Maps are generated by moving the stage, instead of shifting the image, auto-focusing was done on blocks of 3×3 pieces and a delay time of five seconds was applied after moving the stage. A more detailed description of this process can be found in subsection 5.2.1 *Image acquisition* on page 45.

Image analysis of mildly stained tissue

The maps generated with *SerialEM* offer an overview of the tissue, while at the same time being detailed enough to identify gold particles. Due to the use of a minimum amount of contrast enhancing agents, it is possible to detect these gold particles with an automated system.

These maps are fed into *FIJI*, where a threshold of 15 is applied, which cuts off every pixel above a brightness value of that³. After that, particles are analysed by roundness, size and skewness, a factor assessing the particle's regularity of brightness. This whole process is summarized in Figure 3.7. To avoid counting clustered gold particles, which can appear by agglomerated secondary antibodies, gold particles in close proximity to each other are excluded.

³The number 15 is an arbitrary unit, it describes a gray value, where 0 is the darkest part and 255 being the lightest part of the image.

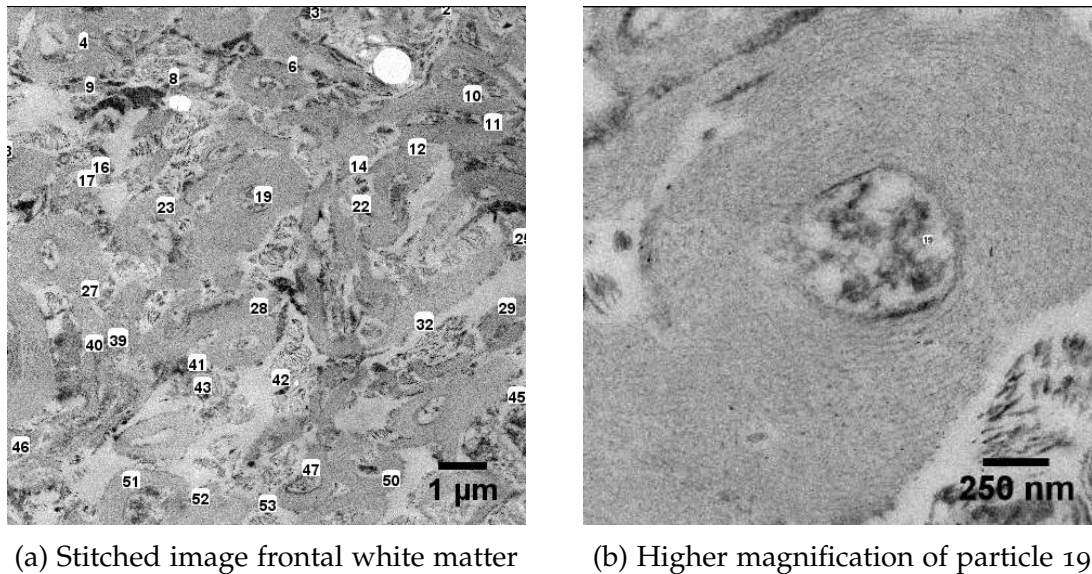


Figure 3.6.: Stitched image of frontal white matter. Gold particles which label ferritin were automatically identified using *FIJI*. These gold particles were labelled with black numbers on a white background. Image **a** shows an overview of a $140 \mu\text{m}^2$ sized stitched image. Image **b** shows a higher magnification of an identified gold particle which was found in the lower center of the picture.

Automatically detected gold particles results

The analysis of gold particles was done on three different brain samples, in each brain the FWM, globus pallidus (GP) and putamen (Put) were examined. The results for each brain and region specimen can be seen in Figure 3.8.

Apparent differences in ferritin concentration can be seen between the different brain regions. FWM showed an average of 49 ferritin proteins per $100 \mu\text{m}^2$ of tissue, while GP and Put showed 95 and 90, respectively. This aligns with findings of ferritin content already discussed in section 2.1 *Sample preparation* on page 7, which showed similar distribution of H-chain ferritin⁴.

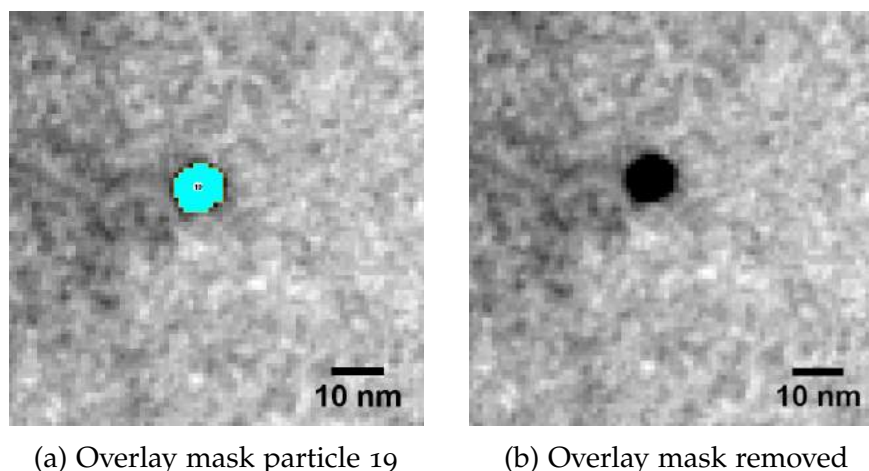
The difference in ferritin concentrations is high between brains, especially if brain 1 and 2 are compared to brain 3. It is also surprising, that brain 1 contains more ferritin in its FWM, than in its GP. These circumstances will be discussed in more detail in section 4.2.2 *Ferritin in different brain regions* on page 39.

Testing nickel grids

Many protocols suggest the use of nickel grids for immunogold labelling, because copper grids tend to oxidise over time. However, oxidation could not be observed on any copper grids, even after five months.

To check for differences in the labelling rate, copper grids were tested against nickel grids. As expected, no significant difference could be seen between the materials. However, nickel grids were easier to handle during labelling, requiring the use of non-magnetic tweezers, but were less susceptible to bending than copper grids, whereas copper grids are cheaper and non-magnetic.

⁴Approximately twice as much ferritin in GP and Put, compared to FWM.



(a) Overlay mask particle 19

(b) Overlay mask removed

Figure 3.7.: Stitched image of frontal white matter. Gold particles were labelled with black numbers on a white background. An overlay mask, seen in image a, shows which part of the particle was identified. Image d shows the gold particle without the overlay mask.

In nickel grids, 39 and 37 ferritin proteins were detected in $100 \mu\text{m}^2$ of FWM for brain 1 and brain 2, respectively. The tests were performed simultaneously with the labelling experiments outlined above. Since this is almost half the labelling rate that was achieved with copper grids (91 and 82 detected ferritin proteins per $100 \mu\text{m}^2$ of FWM for brain 1 and brain 2, respectively), compare Figure 3.8, nickel grids don't seem to have an overall positive impact on ferritin labelling.

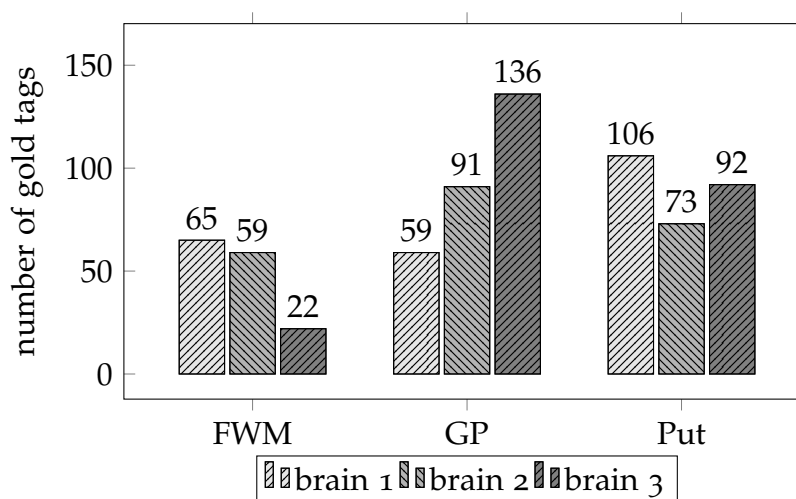


Figure 3.8.: The graph shows gold particles detected per brain region. Brain regions: FWM = frontal white matter, GP = globus pallidus, Put = Putamen. The height of the column represents the number of gold particles found per $100 \mu\text{m}^2$ of tissue. Gold particles indicate ferritin by binding via a secondary antibody to a formerly applied primary anti ferritin H-chain antibody.

3.5. Analytical electron microscopy results

Ferritin is labelled with an antibody, which is tagged with a 10 nm gold particle, so the iron core inside of ferritin should be found in close proximity to this

gold particle. This circumstance is investigated using specialized TEM techniques, namely EFTEM and EDX.

3.5.1. EFTEM results

The location of iron can be seen in Figure 3.9b where an iron M-map⁵ was generated with inverted colors. Iron cores can be seen as black dots⁶, because the brightness of a pixel is indirectly proportional to the strength of the signal. Since the immunogold particles are easily visible in conventional TEM, see Figure 3.9a, ferritin iron cores can be associated with these gold particles. A close up look in Figure 3.9d reveals, that gold is still visible in the iron M-map. This is due to a crosstalk between the iron and gold channel, both absorbing energy in the range of 54 eV.

Many other metals, such as osmium, also absorb in the same energy range as the M-edge of iron [33], making other structures in the sample visible as well. This challenge is addressed by locating iron in a different energy range, the L-edge, which is seen in Figure 3.9c. This energy range is specific to only iron and not found in other metals and can therefore be considered as reliably locating iron. However, due to the energy absorption in a higher energy range, the signal received from the L-edge is lower than the signal received from the M-edge.

3.5.2. EDX results

EDX was used in this thesis to investigate the elemental composition of small areas. This technique is used as a second approach, in order to confirm the results from EFTEM measurements.

EDX measurements are done in STEM mode, see section 2.5.3 *Scanning transmission electron microscopy* on page 20, hence, images acquired in this mode are displayed in inverse colors, see Figure 3.10a. In these images, elemental analysis is done by firstly selecting a small area, in this case the gold or iron particle. Then, X-rays are acquired at the detector for a defined period of time and energy range, while the electron beam is scanning the chosen area. In Figure 3.10a those chosen areas can be seen: the gold particle (1) was indicated by a red box, putative iron cores (2,3) are enclosed in blue boxes. A reference area (4), which is necessary to define a background signal, is enclosed in a white box.

The results of these EDX measurements are plotted in graphs, which can be seen in Figure 3.10c. The location of the peak on the x-axis defines the energy of the peak in keV. These observed energies can be correlated to different elements, since every element emits X-rays in characteristic wavelengths, see also 2.5.1. The peaks, indicated by red arrows in area 1, correlate to energy levels present in gold, while the peaks in area 2 and 3, indicated by a blue arrow, correlate to iron. The peaks visible in the reference area correlate to copper (white arrow) and other heavy metals used for staining (e.g. Pb further to the left of the spectrum).

⁵The letter M describes the electron shell that was responsible for the energy loss of the incoming electron.

⁶Elemental maps are monochrome negative images. Here, colors were inverted.

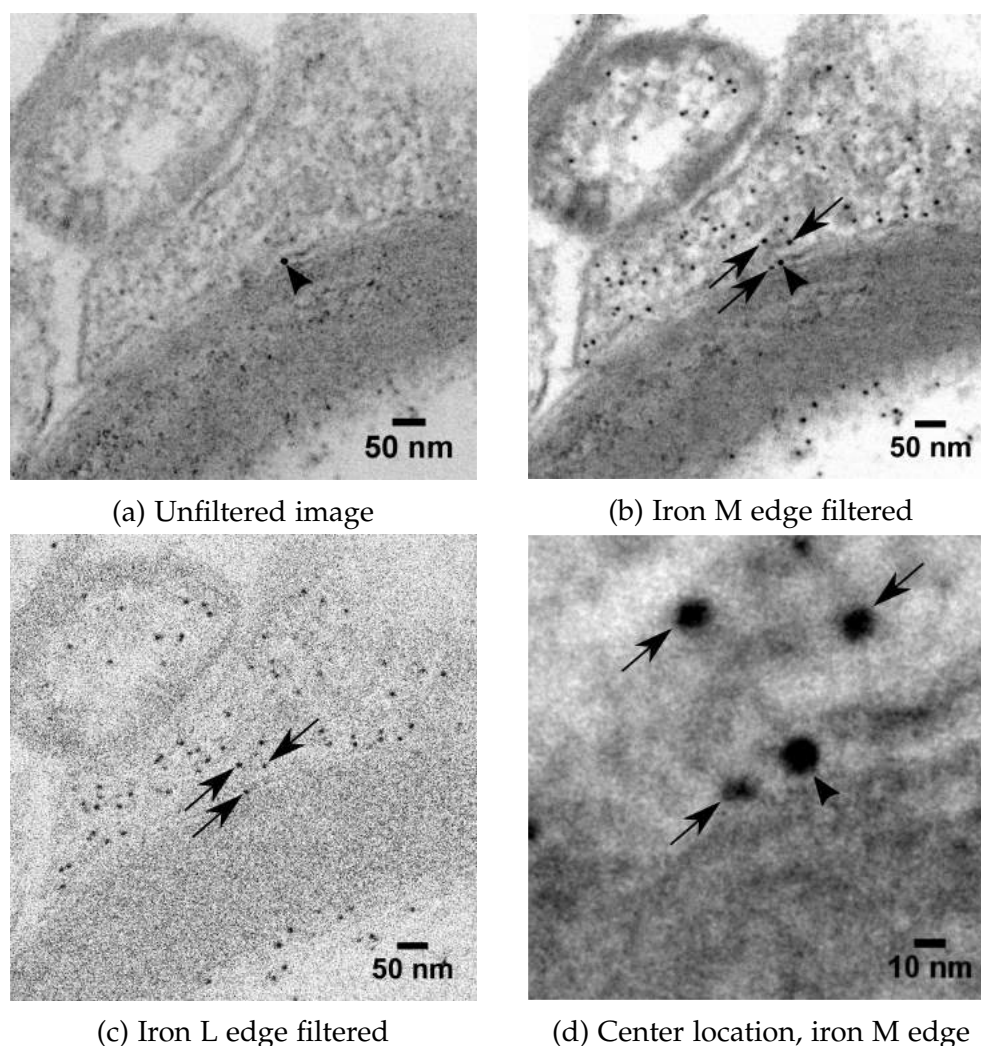


Figure 3.9.: EFTEM elemental map for iron. Image **a** shows an unfiltered overview of the location used for EFTEM analysis. Image **b** shows an iron M-map which was acquired using a three-window approach. Image **c** shows an iron L-map filtered image with less background signal, the gold particle is no longer visible in this energy range. Image **d** shows the center of image **b** in a higher magnification. Iron particles can be seen in images **b**, **c**, **d** as small black dots, indicated by black arrows. In images **a**, **b**, **d**, an immunogold particle can be seen in the centre as a black dot, indicated by black arrowheads. In the centre of images **a**, **b**, **d** an iron particle in close proximity to a gold particle can be seen. All images show an axon surrounded by a myelin sheath, which is on top enclosed by an oligodendrocyte. Images **b**, **c**, **d** are inverted for visibility.

Ferritin iron cores were indeed found near gold particles, see Figure 3.9d, and Figure 3.10. The distance between gold particles and iron cores was usually within 20 nm. This distance is given by the length of two antibodies, spanning between the ferritin protein and the gold particle.

However, not all gold particles could be seen close to an iron core. This could be caused by multiple factors, which are discussed in section 4.3 *Analytical EM* on page 40.

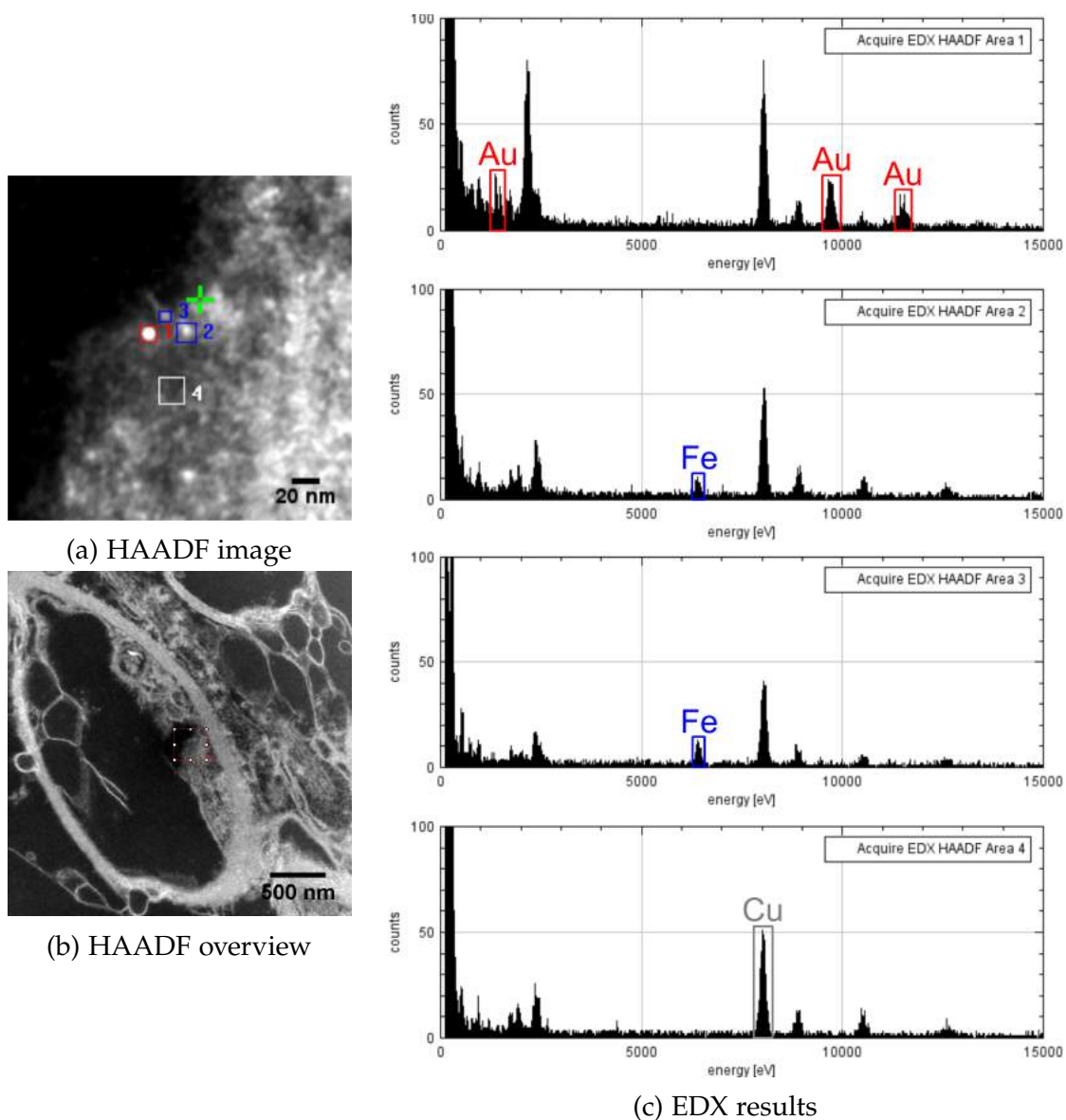


Figure 3.10.: The images were acquired using an HAADF detector, where **a** shows the locations of EDX analysis and **b** shows an overview of the acquired location. The corresponding signals can be seen in image **c**, where the same color for the boxes were used. Area 1 (red box) shows a gold particle, recognizable by its homogeneous, strong signal and peaks at 9.7, 2.1 and 11.4 keV. Areas 2 & 3 (blue boxes) show supposed iron particles, where a characteristic iron peak is observed at 6 keV. Area 4 (white box) shows a reference area, where a strong copper peak at 7.5 keV is visible.

4. Discussion

This thesis provides a workflow, capable of detecting ferritin in human brain tissue using immuno-EM. Several attempts at improving the embedding and fixation method for this endeavour, as well as for the process of labelling and analysis, have been undertaken. The next sections assess these attempts and argue for or against their use in upcoming experiments.

4.1. Fixation and embedding refinement

Different fixation and embedding methods were tested for human brain tissue. Results showed that the slightly modified standard in-house fixation and embedding protocols worked best for the task of processing human brain tissue for immuno-EM. The use of LR-white for embedding samples was a rather uncomplicated process, mainly due to the low toxicity of LR-white [47] and the use of LR-white for embedding at room temperature, as well as the simple polymerization process.

Using low amounts of fixative for immunogold labelling usually results in loss of ultrastructural detail. However, it is strongly suggested that tissue structure and quality was already heavily compromised before the samples were chemically fixed¹. This can be attributed to the samples suffering immensely from autolysis, due to the long time frame between death and fixation of the brain. Autolysis is rapidly degrading brain tissue after death, leading to swelling of cells and breakdown of membranes [60].

Reduced tissue quality due to autolysis was a heavily limiting factor in cell identification, therefore, no cell specific ferritin identification was executed. This problem was postponed for upcoming research, since cell specific ferritin identification is a key part of this research. However, in future projects, cells could be identified via cell specific markers, such as *Myelin oligodendrocyte glycoprotein* for the identification of oligodendrocytes [61].

Furthermore, a shorter post mortem time frame would lead to improved tissue quality. This could be achieved by the use of brain tissue from neurosurgery.

4.1.1. Optimal fixation and embedding procedure

The use of 2 % FA and 0.1 % GA were suggested by a number of protocols. The fixation procedure is both easy and safe, due to the use of low amounts of fixative. This suggests that the process of fixation can be used for future experiments without any modifications.

¹Sele, 2018 personal communication

The tests with PIPES buffer for fixation did not give positive results in terms of antigenicity, however, it contributed to a better fixation quality for lipids. Lower concentrations of PIPES, e.g. 2 % PIPES and 2 % FA could theoretically result in acceptable antigenicity. A better fixation of lipids would also help the identification of cells. If time and resources are available, further research should be conducted in the use of PIPES buffer in these experiments.

The amount of osmium for mildly contrasted tissue was chosen to be 0.1 % OsO_4 , because neither the fixation of tissue, nor the contrast improved with the quadruple amount of osmium.

Neither the use of 100 %, nor the exclusion of oxygen during polymerization can be seen as successful experiments and should therefore not be used in future experiments. The repetition of these experiments is discouraged, because the anticipated benefits could not be met in any ways.

4.2. Immunogold labelling

Tests with different concentrations of primary antibody resulted in a reliable labelling workflow for ferritin in human brain tissue. The use of a *Bioss* primary antibody dilution of 1:50 gave the best results and was used in subsequent experiments.

The labelling method used here, also called post embedding labelling, is capable of targeting the antigens of ferritin proteins on the surface of the tissue. This reduces the idealistic labelling rate, where every ferritin in the tissue is labelled, to around 5 %. This raw estimate is derived from the circumstance, that most ferritin is inaccessible to antibodies, because the protein is only 10 nm in diameter, however statistically distributed in a 70 nm thick slice, see also Figure 4.1. Only ferritin antigens present on the surface can be tagged by an antibody and labelled with a gold particle. This is the reason why so many unlabelled ferritin iron cores can be seen in Figure 3.9b.

Even though only small numbers of ferritin can be detected, this workflow allows the preparation and analysis of large amounts of tissue in relatively short amounts of time. Furthermore, the number of ferritin detected per area is statistically irrelevant, if a low ferritin count is balanced by a larger area acquired.

4.2.1. Detecting ferritin in heavily stained tissue

Cell structures, especially membranes and cell borders could be identified much more easily when a higher amount of contrast enhancing agents were used (Pb-citrate 15 min, platinum-blue 7 min, 1 % OsO_4 2 hours). This allowed localising gold particles in a way in which ferritin could be ascribed to specific cells. However, due to the autolytic tissue used for these experiments, many cells could not be reliably identified. Therefore, a cell specific analysis of ferritin was not performed here.

4.2.2. Detecting ferritin in mildly stained tissue

Tissue that had been incubated in lower amounts of contrast enhancing agents (Pb-citrate 30 s, 0.1 % OsO₄ 2 hours) allowed the fast and reliable detection of ferritin, even in an automated fashion. Large areas of tissue could be acquired in a semi-automated fashion using *SerialEM*. Afterwards, these automatically acquired images are automatically analysed for gold particles using *ImageJ*.

This approach at localising and quantifying iron has the advantage of being able to analyse a large sample size in a relatively short time, compared to manual analysis. However, the low contrast in the tissue makes it hard to identify individual cells. This could change, if brain tissue with fewer signs of autolysis is acquired. It is expected, that tissue with better quality could allow for cell specific ferritin identification, even with low amounts of fixative and contrast enhancing agents.

Improving the automatic detection of gold particles

In the sample, the contrast provided by the gold particle was good enough to be distinguished from surrounding tissue most of the time. However, some parts of the tissue showed similar contrast to gold particles. These areas can come from osmium or lead precipitations which can be confused with gold particles.

Most of these false positives were excluded from the automated gold particle count because their shape is not round. The shape of immunogold particles is precise and round and thus they can be automatically distinguished from other particles.

Other, round false positives could be removed, because the majority of these particles did not have an even distribution of brightness values, compared to gold particles. This was done with the factor skewness, which assesses this property of a particle. Since gold particles are evenly shaped and made solely from gold, they possess a high skewness. Particles with a low skewness could be removed from being counted as gold particles.

Furthermore, clustered gold particles, emerging from agglomerations of secondary antibodies, could be removed by hand. These steps made the automatic identification of gold particles almost as reliable as counting per hand. This automated identification could be done in seconds, compared to manually counting gold particles, which takes a few minutes per image and is a rather undesirable task.

Ferritin in different brain regions

Regarding the analysis of ferritin in different brain regions, as seen in Figure 3.8, this workflow also allowed comparing the amount of ferritin between different brain regions. This thesis is not trying to investigate the differences in ferritin content in brain regions, but rather provide a workflow for doing exactly this. Therefore, a statistical analysis of the ferritin content was not undertaken.

The distribution of ferritin in the different brain regions aligns well with what we expected to find. Approximately twice as much ferritin can be found in GP and Put, compared to FWM, if the mean value is calculated on the basis of three brains. A further statistical analysis was not undertaken because of the low number of

samples. Interestingly, FWM in brain 1 showed a high amount of ferritin compared to the GP (65 gold particles per $100 \mu\text{m}^2$ vs. 59 gold particles per $100 \mu\text{m}^2$) This may be due to a statistical error and will be further investigated in future experiments. Since the generated data overall aligns well with previous findings of ferritin in human brain tissue with different methods (see section 2.1 *Sample preparation* on page 7), it can be assumed that the workflow proposed in this thesis works reasonably well.

4.2.3. Negative Controls

The use of a negative negative controls for each type of tissue showed a constant 5 % gold background, which was acceptable for experiments performed in this thesis. Gold background did not differ significantly between tissue used for tissue specific ferritin labelling and cell specific ferritin labelling, since both workflows shared mostly similar embedding techniques.

Isotype controls showed a similar gold background as negative controls, which was around 5 %. This suggests that the primary antibody is specific for labelling ferritin, since isotypes of the anti-ferritin antibodies did not target unspecific structures of the tissue. Dividing the number of gold granules in the tissue samples by the number of gold granules in the negative controls results in a signal to noise ratio of 20:1, so it can be assumed that the labelling procedure used for these experiments provided a specific labelling of ferritin.

4.3. Analytical EM

A further step of confirming the validity of the method was performed with analytical EM. This confirmed that ferritin iron cores are found close to gold particles.

Elemental maps generated with EFTEM revealed a close proximity of gold particles near these iron cores. This confirms the specificity of labelling ferritin with immunogold.

The vast majority (~90 %) of gold granules was found within 20 nm to an iron core. However, some gold particles could not be found in the range of 20 nm.

Those gold particles that were not close to an iron core were either unspecific (i.e. they belonged to the 5 % background), or they labelled an empty ferritin core (as explained in Figure 4.1) or it is also possible that the gold particle masks the ferritin iron core by sitting on top of the protein. A rough estimate of ferritin iron cores that were either empty or masked by gold particles is ~10 % of total ferritin iron cores found. This brings the total number of falsely identified ferritin to ~10 %, when the gold background is subtracted.

Because EFTEM is susceptible to errors ranging from badly adjusted instruments to overlap of edges leading to false positives, as a second measure to confirm EFTEM results, EDX was used. EDX could also verify that most ferritin iron cores can be seen near gold particles. Furthermore, EDX could demonstrate that the highly visible, dark/round spots in the images are indeed immunogold particles.

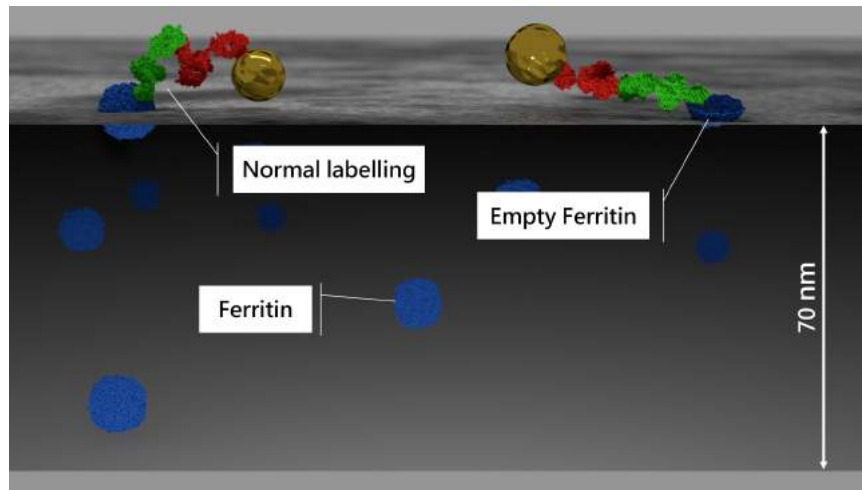


Figure 4.1.: Possible causes for ferritin cores that cannot be identified via EFTEM or EDX. This image shows a scheme of a side view from a sample tagged labelled with immunogold. On the left a possible scenario is shown, where the ferritin particle is cut in a fashion that excludes the iron core of the protein, while the protein hull remains available for antibody tagging. To the right a ferritin particle can be seen, which is blocked in the vertical axis by a gold particle of bigger size. Furthermore, on the bottom it is shown how most ferritin iron cores can be seen in EFTEM, however they cannot be labelled with an antibody, since they are not presenting antigens on the surface of the sample.

This clearly demonstrates that post-embedding labelling of ferritin in human brain tissue is indeed a reliable technique.

4.4. Conclusion

The workflow established in this thesis enables accurate, fast and easy detection of ferritin in human brain tissue. The specificity of ferritin detection was not only validated using two types of negative controls, but also by two independent and highly accurate analytical EM techniques.

Even though it was not possible to provide a single workflow that can both detect ferritin automatically and with high accuracy in cells, these two workflows proved to be successful.

One of the biggest challenges was to deal with autolysis in the human brain tissue samples. Autolysis made it difficult to distinguish cell types from each other and should be addressed in a further study.

4.5. Outlook

This thesis provides a solid workflow which can be used in larger experiments. This enables comparing different brain regions for their cell and tissue specific ferritin load. Furthermore, the information of ferritin concentrations can be compared and correlated to the iron load in the same tissues using EFTEM experiments, which are done by our group.

After gaining enough information on healthy brain tissue and perfecting the

workflows, experiments can be performed on AD brain tissue. Comparing deceased brain tissue to healthy brain tissue allows to highlight differences in ferritin and iron loads between brain areas and cell types in these areas. This could help to provide a better understanding of some neurodegenerative diseases and their correlation with brain iron overload, as well as the role that ferritin plays in situation.

5. Experimental

Experiments were performed from 1. August 2017 until 2. July 2018 at the Medical University of Graz, department of Cell Biology, Histology and Embryology. Chemicals and devices used in this thesis can be found in the Appendix A *Materials* on page 49. Samples obtained from autopsy are in accordance with the ethics department of the medical university of Graz votum number 28-549 ex 15/16. Samples were chemically fixed and embedded according to modified in-house protocols.

5.1. Sample Preparation

Human brain tissue was obtained from 8 patients during autopsy at the department of pathology. Three of these brains (number Fe270217, Fe171031 & Fe171103, see Table 5.1) were used for experiments. These three brains are referred to as brain 1-3 in this thesis. Time between death and autopsy ranged from eight to 24 hours, see Table 5.1. Brain regions obtained for experiments included frontal white matter (FWM), putamen (Put) and globus pallidus GP). Samples were stored in saline until further processing.

Table 5.1.: Brain samples obtained from autopsy. Sorted by date received. In-house number includes date received. Time until fixation represents time between the persons death and start of the fixation process.

number		time until fixation [HH:MM]	age	gender
in-house	autopsy			
Fe270217	272/17	09:10	72	m
Fe171031	P2017901217	15:58	61	f
Fe171103	P2017901232	18:05	69	f
Fe180206-59	159/18	19:50	70	
Fe180206-60	160/18	20:55	53	
Fe180223	246/18	23:40	81	m
Fe180323	386/18	20:00	86	m
Fe180326	399/18	15:30	74	f

5.1.1. Fixation

Human brain tissue obtained from autopsy was immediately cut into approximately 1 mm³ cube shaped pieces and fixed in a solution of 0.1 % glutaraldehyde (GA) and 2 % formaldehyde (FA) for six hours. Specimens were subsequently placed in phosphate buffer (PB) for storage at 4 °C, until further use.

After being washed twice in 0.1 M PB for 5 min, samples were treated with 0.15 M OsO_4 (or 0.1 m/v%) combined with 0.15 M $\text{K}_3\text{Co}(\text{CN})_6$ in an aqueous solution for 2 hours. It is advantageous to move the samples during fixation, e.g. on a shaker to ensure maximum penetration. After that, samples were washed with 0.1 M PB thrice, followed by a washing step of 2 times ddH₂O for 5 min each.

5.1.2. LR-White Embedding

After fixation, samples were dehydrated in a graded EtOH series of 50 % EtOH and 70 % EtOH for 30 min each. Subsequently, samples were treated with pure LR white for one hour, followed by LR white over night and another change of LR white for one hour the next day.

Thereafter, samples were encapsulated in gelatin capsules, obtained from *Groep Christine Electron Microscopy Supplies, Tulln, Austria*. Capsules were filled to the top with LR white and sealed airtight. For identification purposes, numbers printed on cellulose paper, can be added to the inside of the capsule. LR white is polymerized at 50 °C for 48 hours in a laboratory-type drying cabinet. After polymerization has occurred, samples are decapsulated, mounted in a sample holder and stored at room temperature (RT) until further use.

5.1.3. Specimen sectioning

The front ends of samples are trimmed to a size of 1 mm² using a mechanical trimmer by *Leica*. Afterwards, 250 nm semi-thin cuts are generated using a *Leica* Ultra-microtome UC-7 fit with in-house glass blades. Slices are transferred onto glass slides and stained using an aqueous 1 % toluidine-blue solution. Staining enables identifying areas of interest in a light microscope. The specimen is trimmed by hand to the area of interest (approximately 0.1 × 0.1 mm in size), using razorblades.

Subsequently, ultra-thin cuts at ~70 nm are obtained using a 45 ° *diatome* diamond knife with a cutting angle at 5 ° and a cutting speed of 0.8 mm/s. Sections are subsequently transferred onto 300 mesh¹ copper grids and dried on filter paper. Thereafter, finished grids are stored on *Plano* silicon holding plate inside a watch glass, for 24 hours to get rid of any remaining moisture. Grids are finally stored in a *Leica* grid box until immunogold labelling is done.

5.1.4. Immunogold labelling

Sections on grids are placed on drops of goat serum blocking solution for 30 min after being washed with PBG twice for 5 min each. Primary antibody (*Bioss* rabbit anti-ferritin H-chain, polyclonal) in a 1:50 diluted PBG solution is applied for 2 h. After washing with PBS four times for 5 min each, a secondary antibody (*Bioss* goat anti-rabbit linked to a 10 nm gold particle) in a 1:100 diluted PBG solution is applied for 1 h. Specimens are washed with PBS four times for 5 min and thrice with ddH₂O for 5 min each. Finally, specimens are dried using filter paper.

¹Mesh size describes the number of horizontal and vertical struts in one inch.

Negative control specimens experience the same process, but no primary antibody solution is applied. Isotype control specimens are treated with a 1:1000 diluted solution of rabbit IgG (*Daco*) instead of applying the primary antibody.

5.1.5. Sample Staining

After drying in a watch glass, samples were either stained for 30 seconds with 3 % Pb-citrate (mildly stained tissue) or with Pb-citrate for 15 min and platinum-blue for 7 min (heavily stained tissue).

Mild staining is done using a ready to use mixture. A droplet of said mixture is applied on parafilm inside a watch glass. Solid NaOH pieces are placed inside the watch glass to prevent the Pb-citrate from reduction. After that, grids are placed onto the Pb-citrate droplet, slices facing the droplet, in for 30 sec. After staining, samples are dried with filter paper, washed in ddH₂O six times, dried and subsequently stored in a grid box until further use.

Heavy staining is done using a *Leica* auto-stainer.

5.2. Transmission Electron Microscopy

Electron microscopic experiments were performed using a *FEI Tecnai G2 20* 120 kV with LaB₆ cathode and a *Gatan Quantum 963 KU Gatan Imaging Filter (GIF)* for EFTEM and EELS as well as an *EDAX EDX Si(Li)* detector for EDX experiments. The *FEI Tecnai G2 20* is fitted with a *Gatan Ultrascan camera* and a *Gatan high angle annular dark field detector*. Further electron microscopic experiments were performed with a *Zeiss EM 900* at 80 kV

5.2.1. Image acquisition

Two areas of interest are selected in the sample using the polygon function of *serialEM* version 3.6. Areas of interest are, on average, the size of 140 μm². These areas are scanned and stitched, using the map generating function of *serialEM*. After baking the area of interest for 10 min with a reduced beam and 5 min with a more intense beam at a magnification of 1.700x, maps are acquired at 10 min 11.500x. Exposure time for image acquisition is performed automatically and lies between 0.5-1 s.

5.3. Image Analysis

Images are analysed using *FIJI* version 1.51r. Here, a threshold from 0 to 15 is applied, excluding all areas of the image that are brighter than 15. This way, gold particles are easily distinguishable from the rest of the tissue. Using the function *Analyze Particles* with setting shown in Table 5.2, gold particles are localised, counted and listed. Generating an overlay mask marks particles in the image itself, so gold particles can be verified by hand.

Table 5.2.: Options and values for *FIJI's Analyze Particles* function

Option	Value
Size (pixel ²)	50-100
Circularity	0.9-1
Show	Overlay Mask
Display results	Yes
In situ Show	Yes

5.4. Analytical EM

Verification of gold and iron particles on images acquired with TEM is done via EFTEM and EDX.

5.4.1. Energy filtered transmission electron microscopy

Energy filtered transmission electron microscopy was performed at 200 kV. Samples were cooked in the electron beam twice for 15 min at 350x and 1800x magnification, subsequently. After gain references were acquired and filter tuning was completed, filtered images were acquired at 80.000x magnification. Before each image acquisition, the zero loss peak was adjusted accordingly.

Energy filtering was performed for the core loss of the iron M-edge at 54 eV with a slit width of 8 eV post-edge and a pre-edge at 50 eV with a slit width of 10 eV. The pre-edge is subsequently subtracted from the post edge for better image quality. In the same fashion, the iron L-edge is acquired at 708 eV using a slit of 20 eV for the post edge, a pre-edge 1 at 680 eV with a slit with of 10 eV and a pre-edge 2 at 680 eV with a slit with of 10 eV.

5.4.2. Energy dispersive X-ray analysis

Energy dispersive X-ray analysis was performed at 200 kV in STEM mode. An area of interest was scanned using an HAADF detector at 80.000 x magnification. In the acquisition software *TIA* gold and iron particles are marked using boxes. A spectrum is acquired with the following parameters: STEM mode at 200 kV, using 240 s for signal acquisition with a window of 0.2 keV per energy slit. Peaks are identified with the *TIA-peak identifier*.

Appendix

Appendix A.

Materials

Table A.1.: This table shows all chemicals which were used in this thesis, sorted alphabetically. The product ID is either the identification number that the company uses to identify its chemicals, or the CAS number if no other information is found.

chemical/name	company	LOT or CAS
ethanol 96 %	AustrAlco	603-202-00-5
glutaraldehyde 95 %	ROTH	3778.1
$K_4(Co(CN)_6)$	Arcos	203920050
lead citrate 3 %	Leica	D170221
lead citrate 3 %	Science services	171117-11
LR-White medium grade	London Resin Company	9262
NaN_3	MERCK	K20135088
NaOH	MERCK	1.06469.1000
PBS pH=7.4	gibco	10010-015
p-formaldehyde 95 %	Sigma Aldrich	441244
platinum-blue	IBI-Blue	IBI080713
toluidin-blue	Fluka	6586-04-5
Tween 20	MERCK	8.22184.0500

Table A.2.: Antibodies used for experiments in this thesis.

company	antibody	LOT
abcam	anti-Ferritin Heavy Chain IgG	ab81444
Bioss	anti-Ferritin Heavy Chain IgG	bs-5907R
british-biocell	goat anti-rabbit IgG 10 nm immunogold	EM.GAR10

Table A.3.: This table shows all devices which were used for experiments in this thesis. Electron microscopes are not found in this table, they are described in detail in chapter 5 *Experimental* on page 43.

device	product name	annotations
auto stainer	Leica EM AC20	
diamond knife	Diatome	size 3 angle 45 °
distillation apparatus	Heraeus Destamat	
glass slides	Assistent ELKA	No. 2406
	Thermo Scientific	Superfrost Plus
glow discharger	Pelco easiglow	Model 91000
grid box	Leica B801003080	
grids	science services no.100	copper 300 square
	agar scientific G2300N	nickel 300 square
light microscopes	Olympus BX41	
mikrotomes	Microm HM 440E	sliding microtome
	Microm HM 355S	rotation microtome
	Leica EM UC6	ultra microtome
pH-measurements	Thermo Orion 3Star	TRIS-Elektrode
pipetts	Eppendorf Research	100-1000 μ l
		20-200 μ l
		2-20 μ l
		0.5-10 μ l
scales	Kern GS	d=0.01 g
	Sartorius Secura	d=0.01 mg
	225D-ICEU	
trimming device	Leica EM Trim2	number 120545 12
silicon holding plates	Plano 10524	

Appendix B.

Addendum

B.1. Code

Listing B.1: Code written in Jython v 1.51w. String a and b are defined to choose the collection of images to stitch. Variables x and y are defined as the number given to the image e.g: for number 14 $x = 4$, $y = 1$. Grid/Collection stitching is done in a snake by rows order with the given grid size. The definitions fusion method, regression threshold, avg displacement threshold, absolute displacement threshold, subpixel accuracy, computation parameters and image output was left on default. After stitching, images are saved into a new directory, adding the number yx automatically.

```
import os
from ij import IJ

number = map(str, range (a,b))
collection = map(str, range (1,6))

for y in number:
    for x in collection:

        IJ.run("Grid/Collection stitching",
            "type = Grid: snake by rows order = Right & Down
            grid_size_x=4 grid_size_y=4 tile_overlap=20
            first_file_index_i=11 directory="directory" + "name" + y + x
            fusion_method=[Linear Blending] regression_threshold=0.30 max/
            avg_displacement_threshold=2.50
            absolute_displacement_threshold=3.50 subpixel_accuracy
            computation_parameters=[Save memory (but be slower)]
            image_output=[Fuse and display]")

        IJ.save("new_directory" + y + x)
        imp = IJ.getImage()
        imp.close()
```


Bibliography

1. Cairo, G., Bernuzzi, F. & Recalcati, S. A Precious Metal: Iron, an Essential Nutrient for All Cells. *Genes & Nutrition* **1**, 25–39. ISSN: 1555-8932 (Mar. 2006) (cit. on p. 1).
2. Genova, M. L. *et al.* The Site of Production of Superoxide Radical in Mitochondrial Complex I Is Not a Bound Ubisemiquinone but Presumably Iron–Sulfur Cluster N2. *FEBS Letters* **505**, 364–368. ISSN: 0014-5793 (Sept. 2001) (cit. on p. 1).
3. Gupta, C. P. Role of Iron (Fe) in Body. *IOSR Journal of Applied Chemistry (IOSR-JAC)* **7**, 38–46 (2014) (cit. on p. 1).
4. Gropper, S. S. & Smith, J. L. *Advanced Nutrition and Human Metabolism* en. ISBN: 978-1-133-10405-6 (Cengage Learning, June 2012) (cit. on p. 1).
5. Theil, E. C. Ferritin: Structure, Gene Regulation, and Cellular Function in Animals, Plants, and Microorganisms. *Annual review of biochemistry* **56**, 289–315 (1987) (cit. on pp. 1, 2).
6. Youdim, M. B. H. & Green, A. R. Iron Deficiency and Neurotransmitter Synthesis and Function. en. *Proceedings of the Nutrition Society* **37**, 173–179. ISSN: 1475-2719, 0029-6651 (Sept. 1978) (cit. on p. 1).
7. Lozoff, B. & Georgieff, M. K. Iron Deficiency and Brain Development. eng. *Seminars in Pediatric Neurology* **13**, 158–165. ISSN: 1071-9091 (Sept. 2006) (cit. on p. 1).
8. Connor, J. R. & Menzies, S. L. Relationship of Iron to Oligodendrocytes and Myelination. *Glia* **17**, 83–93 (1996) (cit. on p. 1).
9. Mizuno, S., Mihara, T., Miyaoka, T., Inagaki, T. & Horiguchi, J. CSF Iron, Ferritin and Transferrin Levels in Restless Legs Syndrome. en. *Journal of Sleep Research* **14**, 43–47. ISSN: 1365-2869 (cit. on p. 1).
10. Hallgren, B. & Sourander, P. The Effect of Age on the Non-Haemin Iron in the Human Brain. en. *Journal of Neurochemistry* **3**, 41–51. ISSN: 0022-3042, 1471-4159 (Oct. 1958) (cit. on p. 1).
11. Dusek, P. & Schneider, S. A. Neurodegeneration with Brain Iron Accumulation. en-US. *Current Opinion in Neurology* **25**, 499. ISSN: 1350-7540 (Aug. 2012) (cit. on p. 1).
12. Schneider, S. A. Neurodegeneration with Brain Iron Accumulation. en. *Current Neurology and Neuroscience Reports* **16**, 9. ISSN: 1528-4042, 1534-6293 (Jan. 2016) (cit. on p. 1).
13. Michaeli, S. *et al.* Assessment of Brain Iron and Neuronal Integrity in Patients with Parkinson’s Disease Using Novel MRI Contrasts. en. *Movement Disorders* **22**, 334–340. ISSN: 1531-8257 (Feb. 2007) (cit. on p. 1).

14. Martin, W. R. W., Wieler, M. & Gee, M. Midbrain Iron Content in Early Parkinson Disease: A Potential Biomarker of Disease Status. en. *Neurology* **70**, 1411–1417. ISSN: 0028-3878, 1526-632X (Apr. 2008) (cit. on p. 1).
15. W, C., Mw, M., Cp, L., A, S. & I, M. Iron Deposits Surrounding Multiple Sclerosis Plaques. eng. *Archives of pathology & laboratory medicine* **106**, 397–399. ISSN: 0003-9985 (Aug. 1982) (cit. on p. 1).
16. Lovell, M., Robertson, J., Teesdale, W., Campbell, J. & Markesbery, W. Copper, Iron and Zinc in Alzheimer's Disease Senile Plaques. en. *Journal of the Neurological Sciences* **158**, 47–52. ISSN: 0022510X (June 1998) (cit. on p. 1).
17. Plascencia-Villa, G. *et al.* High-Resolution Analytical Imaging and Electron Holography of Magnetite Particles in Amyloid Cores of Alzheimer's Disease. en. *Scientific Reports* **6**, 24873. ISSN: 2045-2322 (Apr. 2016) (cit. on p. 1).
18. Masters, C. L. *et al.* Amyloid Plaque Core Protein in Alzheimer Disease and Down Syndrome. en. *Proceedings of the National Academy of Sciences* **82**, 4245–4249. ISSN: 0027-8424, 1091-6490 (June 1985) (cit. on p. 1).
19. Kell, D. B. Towards a Unifying, Systems Biology Understanding of Large-Scale Cellular Death and Destruction Caused by Poorly Liganded Iron: Parkinson's, Huntington's, Alzheimer's, Prions, Bactericides, Chemical Toxicology and Others as Examples. en. *Archives of Toxicology* **84**, 825–889. ISSN: 0340-5761, 1432-0738 (Nov. 2010) (cit. on p. 2).
20. Smith, M. A., Harris, P. L. R., Sayre, L. M. & Perry, G. Iron Accumulation in Alzheimer Disease Is a Source of Redox-Generated Free Radicals. en. *Proceedings of the National Academy of Sciences of the United States of America* **94**, 9866 (Sept. 1997) (cit. on p. 2).
21. Andersen, J. K. Oxidative Stress in Neurodegeneration: Cause or Consequence. *Nature Reviews Neuroscience* **10**, S18–S25. ISSN: 1471-003X (July 2004) (cit. on p. 2).
22. Harrison, P. M., Fischbach, F. A., Hoy, T. G. & Haggis, G. H. Ferric Oxyhydroxide Core of Ferritin. en. *Nature* **216**, 1188–1190. ISSN: 1476-4687 (Dec. 1967) (cit. on pp. 2, 3).
23. Mann, S., Bannister, J. V. & Williams, R. J. P. Structure and Composition of Ferritin Cores Isolated from Human Spleen, Limpet (*Patella Vulgata*) Hemolymph and Bacterial (*Pseudomonas Aeruginosa*) Cells. *Journal of Molecular Biology* **188**, 225–232. ISSN: 0022-2836 (Mar. 1986) (cit. on p. 2).
24. Berman, H. M. *et al.* The Protein Data Bank. en. *Nucleic Acids Research* **28**, 235–242. ISSN: 0305-1048 (Jan. 2000) (cit. on p. 2).
25. Levi, S. *et al.* Mechanism of Ferritin Iron Uptake: Activity of the H-Chain and Deletion Mapping of the Ferro-Oxidase Site. A Study of Iron Uptake and Ferro-Oxidase Activity of Human Liver, Recombinant H-Chain Ferritins, and of Two H-Chain Deletion Mutants. en. *Journal of Biological Chemistry* **263**, 18086–18092. ISSN: 0021-9258, 1083-351X (May 1988) (cit. on p. 2).
26. Harrison, P. M. & Arosio, P. The Ferritins: Molecular Properties, Iron Storage Function and Cellular Regulation. en. *Biochimica et Biophysica Acta (BBA) - Bioenergetics* **1275**, 161–203. ISSN: 00052728 (July 1996) (cit. on p. 3).

27. Wang, Z. *et al.* Structure of Human Ferritin L Chain. eng. *Acta Crystallographica. Section D, Biological Crystallography* **62**, 800–806. ISSN: 0907-4449 (July 2006) (cit. on p. 3).
28. Friedman, A., Arosio, P., Finazzi, D., Koziorowski, D. & Galazka-Friedman, J. Ferritin as an Important Player in Neurodegeneration. en. *Parkinsonism & Related Disorders* **17**, 423–430. ISSN: 13538020 (July 2011) (cit. on p. 3).
29. Drayer, B. *et al.* Magnetic Resonance Imaging of Brain Iron. en, 8 (1986) (cit. on p. 3).
30. Krebs, N. *et al.* Assessment of Trace Elements in Human Brain Using Inductively Coupled Plasma Mass Spectrometry. en. *Journal of Trace Elements in Medicine and Biology* **28**, 1–7. ISSN: 0946672X (Jan. 2014) (cit. on p. 3).
31. Meguro, R., Asano, Y., Odagiri, S., Li, C. & Shoumura, K. Cellular and Subcellular Localizations of Nonheme Ferric and Ferrous Iron in the Rat Brain: A Light and Electron Microscopic Study by the Perfusion-Perls and -Turnbull Methods. en. *Archives of Histology and Cytology* **71**, 205–222. ISSN: 0914-9465, 1349-1717 (2008) (cit. on p. 3).
32. Pan, Y.-H. *et al.* 3D Morphology of the Human Hepatic Ferritin Mineral Core: New Evidence for a Subunit Structure Revealed by Single Particle Analysis of HAADF-STEM Images. *Journal of Structural Biology* **166**, 22–31. ISSN: 1047-8477 (Apr. 2009) (cit. on p. 3).
33. Funk, D. *Establishment of a Workflow for High Resolution Visualization of Iron Deposits in the Human Brain by Analytical Electron Microscopy* English. June 2018 (cit. on pp. 4, 33).
34. Timms, B. G. Postembedding Immunogold Labeling for Electron Microscopy Using LR White Resin. en. *American Journal of Anatomy* **175**, 267–275. ISSN: 0002-9106, 1553-0795 (Feb. 1986) (cit. on p. 4).
35. Bessis, M. C. & Breton-Gorius, J. Iron Metabolism in the Bone Marrow as Seen by Electron Microscopy: A Critical Review. en. *Blood* **19**, 635–663. ISSN: 0006-4971, 1528-0020 (June 1962) (cit. on p. 4).
36. Connor, J. R., Snyder, B. S., Arosio, P., Loeffler, D. A. & LeWitt, P. A Quantitative Analysis of Isoferritins in Select Regions of Aged, Parkinsonian, and Alzheimer's Diseased Brains. eng. *Journal of Neurochemistry* **65**, 717–724. ISSN: 0022-3042 (Aug. 1995) (cit. on p. 7).
37. Hukkanen, V. & Røyttä, M. Autolytic Changes of Human White Matter: An Electron Microscopic and Electrophoretic Study. *Experimental and molecular pathology* **46**, 31–39 (1987) (cit. on p. 8).
38. Kiernan, J. A. Formaldehyde, Formalin, Paraformaldehyde And Glutaraldehyde: What They Are And What They Do. en. *Microscopy Today* **8**, 8–13. ISSN: 1551-9295, 2150-3583 (Jan. 2000) (cit. on p. 9).
39. Eldred, W. D., Zucker, C., Karten, H. J. & Yazulla, S. Comparison of Fixation and Penetration Enhancement Techniques for Use in Ultrastructural Immunocytochemistry. en. *Journal of Histochemistry & Cytochemistry* **31**, 285–292. ISSN: 0022-1554, 1551-5044 (Feb. 1983) (cit. on p. 9).

40. Watson, M. L. Staining of Tissue Sections for Electron Microscopy with Heavy Metals. en. *The Journal of Cell Biology* **4**, 475–478. ISSN: 0021-9525, 1540-8140 (July 1958) (cit. on p. 9).
41. Lodish, H. *et al.* Biomembranes: Structural Organization and Basic Functions. en. *Molecular Cell Biology*. 4th edition (2000) (cit. on p. 9).
42. Riemersma, J. C. Osmium Tetroxide Fixation of Lipids: Nature of the Reaction Products. en. *Journal of Histochemistry & Cytochemistry* **11**, 436–442. ISSN: 0022-1554, 1551-5044 (May 1963) (cit. on p. 9).
43. Roth, J., Bendayan, M., Carlemalm, E., Villiger, W. & Garavito, M. Enhancement of Structural Preservation and Immunocytochemical Staining in Low Temperature Embedded Pancreatic Tissue. en. *Journal of Histochemistry & Cytochemistry* **29**, 663–671. ISSN: 0022-1554, 1551-5044 (May 1981) (cit. on p. 9).
44. Tamaki, H. & Yamashina, S. Improved Method for Post-Embedding Cytochemistry Using Reduced Osmium and LR White Resin. en. *Journal of Histochemistry & Cytochemistry* **42**, 1285–1293. ISSN: 0022-1554, 1551-5044 (Sept. 1994) (cit. on p. 9).
45. White, D. L., Mazurkiewicz, J. E. & Barnett, R. J. A Chemical Mechanism for Tissue Staining by Osmium Tetroxide-Ferrocyanide Mixtures. en. *Journal of Histochemistry & Cytochemistry* **27**, 1084–1091. ISSN: 0022-1554, 1551-5044 (July 1979) (cit. on p. 10).
46. Tamaki, H. & Yamashina, S. Improved Method for Post-Embedding Cytochemistry Using Reduced Osmium and LR White Resin. en. *Journal of Histochemistry & Cytochemistry* **42**, 1285–1293. ISSN: 0022-1554, 1551-5044 (Sept. 1994) (cit. on p. 10).
47. Sigma-Aldrich. 62662 LR-White Product Information English. 2014 (cit. on pp. 10, 37).
48. Pandithage, R. Brief Introduction to Contrasting for EM Sample Preparation. en (Oct. 2013) (cit. on pp. 15, 16).
49. Inaga, S. *et al.* Platinum Blue as an Alternative to Uranyl Acetate for Staining in Transmission Electron Microscopy. eng. *Archives of Histology and Cytology* **70**, 43–49. ISSN: 0914-9465 (Apr. 2007) (cit. on p. 15).
50. Schermelleh, L., Heintzmann, R. & Leonhardt, H. A guide to super-resolution fluorescence microscopy. en. *The Journal of Cell Biology* **190**, 165–175. ISSN: 0021-9525, 1540-8140 (July 2010) (cit. on p. 16).
51. Schindelin, J. *et al.* Fiji: An Open-Source Platform for Biological-Image Analysis. en. *Nature Methods* **9**, 676–682. ISSN: 1548-7105 (July 2012) (cit. on p. 17).
52. Egerton, R. F. *Electron Energy-Loss Spectroscopy in the Electron Microscope* Third edition. en. ISBN: 978-1-4419-9582-7 978-1-4419-9583-4 (Springer, New York, 2011) (cit. on p. 19).
53. *Energy Dispersive X-Ray Analysis in the Electron Microscope* en. ISBN: 978-0-203-48342-8. doi:10.4324/9780203483428 (Garland Science, July 2003) (cit. on p. 19).

54. Bauer, R. in *Methods in Microbiology* (ed Mayer, F.) 113–146 (Academic Press, Jan. 1988) (cit. on p. 20).
55. Goldstein, J. *et al.* *Scanning Electron Microscopy and X-Ray Microanalysis: Third Edition* 3rd ed. en. ISBN: 978-0-306-47292-3 (Springer US, 2003) (cit. on p. 21).
56. Herrick, J. A. & Kempf, J. E. A Study of the Fungistatic and Fungicidal Properties and of the Toxicity for Mice of Sodium Azide. en, 6 (cit. on p. 23).
57. Eldred, W. D., Zucker, C., Karten, H. J. & Yazulla, S. Comparison of Fixation and Penetration Enhancement Techniques for Use in Ultrastructural Immunocytochemistry. en. *Journal of Histochemistry & Cytochemistry* **31**, 285–292. ISSN: 0022-1554, 1551-5044 (Feb. 1983) (cit. on p. 24).
58. Baur, P. S. & Stacey, T. R. The Use of PIPES Buffer in the Fixation of Mammalian and Marine Tissues for Electron Microscopy. en. *Journal of Microscopy* **109**, 315–327. ISSN: 00222720 (Apr. 1977) (cit. on p. 24).
59. Skepper, J. N. & Powell, J. M. Immunogold Staining of London Resin (LR) White Sections for Transmission Electron Microscopy (TEM). en. *Cold Spring Harbor Protocols* **2008**, pdb.prot5016–pdb.prot5016. ISSN: 1559-6095 (June 2008) (cit. on p. 24).
60. Matakas, F., Cervos-Navarro, J. & Schneider, H. Experimental Brain Death: 1. Morphology and Fine Structure of the Brain. en. *Journal of Neurology, Neurosurgery & Psychiatry* **36**, 497–508. ISSN: 0022-3050 (Aug. 1973) (cit. on p. 37).
61. Scolding, N. J. *et al.* Myelin-Oligodendrocyte Glycoprotein (MOG) Is a Surface Marker of Oligodendrocyte Maturation. *Journal of Neuroimmunology* **22**, 169–176. ISSN: 0165-5728 (May 1989) (cit. on p. 37).